



41 **Abstract**

42 The ForestScan project was conceived to evaluate new technologies for characterising forest structure and biomass at Forest  
43 Biomass Reference Measurement Sites (FBRMS). It is closely aligned with other international initiatives, particularly the  
44 Committee on Earth Observation Satellites (CEOS) Working Group on Calibration & Validation (WGCV) aboveground  
45 biomass (AGB) cal/val protocols, and is part of GEO-TREES, an international consortium dedicated to establishing a global  
46 network of Forest Biomass Reference Measurement Sites (FBRMS) to support EO and encourage investment in relevant field-  
47 based observations and science. ForestScan is the first demonstration of what can be achieved more broadly under GEO-  
48 TREES, which would significantly expand and enhance the use of EO-derived AGB estimates.

49

50 We present data from the ForestScan project, a unique multiscale dataset of tropical forest three-dimensional (3D) structural  
51 measurements, including terrestrial laser scanning (TLS), unpiloted aerial vehicle laser scanning (UAV-LS), airborne laser  
52 scanning (ALS), and in-situ tree census and ancillary data. These data are critical for the calibration and validation of EO  
53 estimates of forest biomass, as well as providing broader insights into tropical forest structure.

54

55 Data are presented for three FBRMS: FBRMS-01: Paracou, French Guiana; FBRMS-02: Lopé, Gabon; and FBRMS-03:  
56 Kabili-Sepilok, Malaysia. Field data for each site include new 3D LiDAR measurements combined with plot tree census and  
57 ancillary data, at a multi-hectare scale. Not all data types were collected at all sites, reflecting the practical challenges of field  
58 data collection. We also provide detailed data collection protocols and recommendations for TLS, UAV-LS, ALS and plot  
59 census measurements for each site, along with requirements for ancillary data to enable integration with ALS data (where  
60 possible) and upscaling to EO estimates. We outline the requirements and challenges for field data collection for each data  
61 type and discuss the practical considerations for establishing new FBRMS or upgrading existing sites to FBRMS standard,  
62 including insights into the associated costs and benefits.

63 **1. Introduction**

64 Our capability to estimate forest structure and AGB has rapidly advanced, leveraging new remote sensing observations from  
65 ground, air, and space. This progress underscores the importance of quantifying and understanding terrestrial carbon sources  
66 and sinks, the response of global forests to climate change, and conservation and restoration efforts at local to global scales.  
67 These new measurements broadly fall into the following categories:

68

69 1) TLS provides highly detailed (centimetre-scale) 3D structural measurements across hectare scales, enabling non-  
70 destructive AGB estimates that are independent of, yet complementary to, empirical allometric model estimates (e.g.  
71 Calders et al., 2022; Demol et al., 2024).

73 2) UAV-LS has evolved from highly specialised and expensive surveying platforms to more operational, low-cost  
74 systems that offer coverage of several to thousands of hectares, with hundreds to thousands of points per square metre  
75 from above. These data can be used to estimate forest canopy height, basal area, tree crown size and shape, vertical  
76 structure, and AGB via allometric model functions of tree properties, including height, diameter at breast height  
77 (DBH), and crown shape (Brede et al., 2022a; Kellner et al., 2019) However, as UAV-LS systems proliferate, the  
78 need for intercalibration between sensors increases, due to differences in scanner and laser properties such as power,  
79 wavelength, divergence, and scan rate, which result in notable variations in penetration and object detection rates  
80 (Vincent et al., 2023).

81 3) Airborne laser scanning (ALS) has been a well-established tool in forestry and forest ecology since the 1990s. ALS  
82 is routinely used to estimate forest height, structure, and AGB at stand level via empirical models and at regional to  
83 national scales via allometric models (Duncanson et al., 2019; Jucker et al., 2017).

84 4) Spaceborne Light Detection and Ranging (Spaceborne LiDAR) (e.g. GEDI, ICESat, and ICESat-2) can provide  
85 estimates of forest height in non-continuous footprints of tens to hundreds of metres, underpinning most large-scale  
86 AGB maps, particularly in the lowland tropics (Avitabile et al., 2011; Avitabile et al., 2016; Saatchi et al., 2011).  
87 Various satellite missions have also provided empirical evidence for correlations between the radar signal and AGB  
88 for  $AGB < 250 \text{ Mg ha}^{-1}$  (Askne and Santoro, 2012), but the ESA BIOMASS mission, launched on the 29<sup>th</sup> of April  
89 2025, is the only mission specifically targeting higher biomass tropical forests (Quegan et al., 2019; Ramachandran  
90 et al., 2023).

91 The current challenge is to consistently collect and process plot-based measurements in support of EO-derived AGB, combine  
92 them, integrate them with long-term ground-based inventory approaches, and optimally use them with EO data. There is  
93 increasing recognition that the value of large-scale EO approaches to assessing AGB and forest structure largely depends on  
94 robust calibration and validation data (Duncanson et al., 2019; Nature Editorial, 2022; Ochiai et al., 2023). This knowledge  
95 and capability gap have led to calls for concerted international funding and coordination to establish long-term Forest Biomass  
96 Reference Measurement Sites (FBRMS), with a particular focus on tropical forests (Labrière et al., 2023; Schepaschenko et  
97 al., 2019).

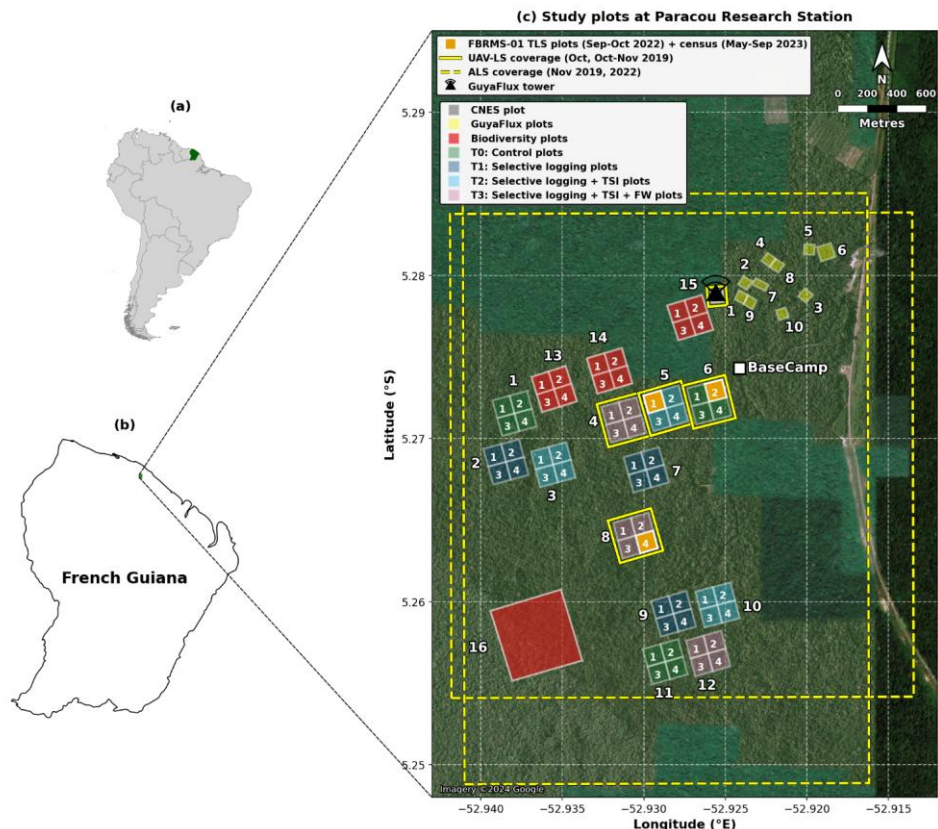
98 102 Here, we present a new dataset from the European Space Agency (ESA) funded ForestScan project, which contributes to this  
99 aim and provides access to data from the first three FBRMS of the GEO-TREES network. The project has collected data,  
100 including TLS, UAV-LS, ALS, and census data, covering three FBRMS across the tropics. We describe these data, related  
101 data collection and processing protocols and tools, and make brief recommendations for future data collection for FBRMS.

106 **2. Methodology**

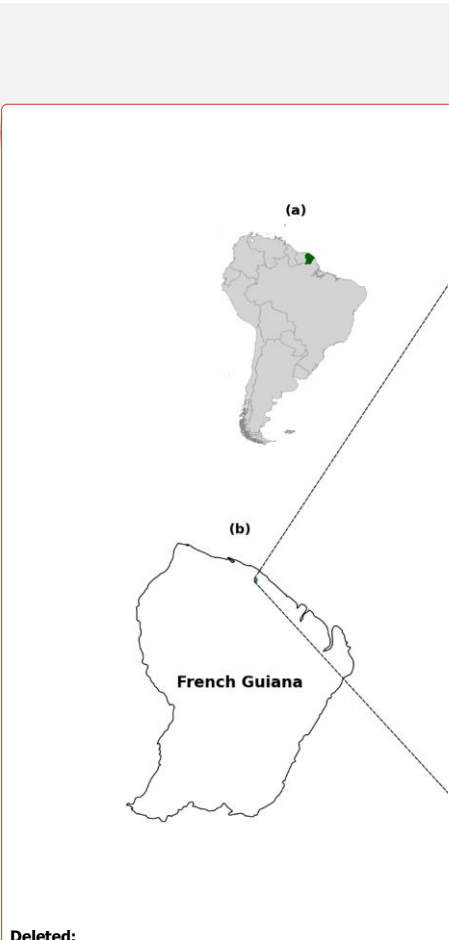
107 **2.1 ForestScan Forest Biomass Reference Measurement Sites (FBRMS)**

108 Three Forest Biomass Research Monitoring Sites (FBRMS) were selected based on various criteria, including the availability  
109 of well-established plots, the representativity of tropical forest types and climates, established collaborations, agreements and  
110 logistical support with in-country partners, and the availability of previously collected data, particularly census data, as well  
111 as ALS and TLS data. The chosen sites were:

112 • FBRMS-01: Paracou Research Station, French Guiana  
113 • FBRMS-02: Station d'Etudes des Gorilles et Chimpanzés, Lopé National Park, Gabon  
114 • FBRMS-03: Kabili-Sepilok, Malaysian Borneo



117 **Figure 1:** Multi-scale map depicting the location and spatial distribution of research plots at Paracou Research Station, French  
 118 Guiana. (a) Location of French Guiana (green) within South America. (b) Location of Paracou Research Station (green) within  
 119 French Guiana. (c) Detailed site map showing the spatial distribution of research plots with treatment-specific colours, UAV-  
 120 LS coverage (yellow solid outline), and ALS coverage (yellow dashed outline). The map displays 15 experimental 4 ha plots,  
 121 each containing four 1 ha subplots numbered 1 - 4 (60 subplots in total; plots 1 - 12: silvicultural treatments; plots 13 - 15:  
 122 Biodiversity monitoring), one large 40 ha Biodiversity plot (plot 16; red), and 10 GuyaFlux plots (yellow). Treatment  
 123 categories include: Biodiversity monitoring plots (plots 13, 14, 15, 16; red), T0 Control (plots 1, 6, 11; green), T1 Selective



**Deleted:** orange

**Deleted:** solid green

127 logging (plots 2, 7, 9; dark blue), T2 Selective logging + thinning by timber stand improvement (TSI; plots 3, 5, 10; cyan), and  
128 T3 Selective logging + TSI + fuelwood harvesting/FW (plots 4, 8, 12; pink). The three FBRMS-01 subplots -FG5c1 (subplot  
129 1 of plot 5), FG6c2 (subplot 2 of plot 6), and FG8c4 (subplot 4 of plot 8)- are shown in solid orange and were surveyed using  
130 terrestrial laser scanning (TLS) with corresponding tree census data. The GuyaFlux tower location is indicated by a black  
131 triangle with radiating transmission waves, and the Base Camp location is marked with a white square. Scale bar: 800 m. Map  
132 data: Natural Earth 10 m cultural vectors. Satellite imagery basemap: Imagery ©2024 Google. Map projection: WGS84  
133 (EPSG:4326).

134

135 The Paracou research station is located near Sinnamary in the northern part of French Guiana, at a latitude of 5°18'N and a  
136 longitude of 52°53'W. It is established on a long-term concession of the French National Centre for Space Studies (CNES)  
137 and is managed by Centre de Coopération Internationale en Recherche Agronomique pour le Développement-Unité Mixte de  
138 Recherche Écologie des Forêts de Guyane (Cirad-UMR EcoFoG). The station experiences an equatorial climate characterised  
139 by two main climatic periods: a well-marked dry season from mid-August to mid-November and a long rainy season, often  
140 interrupted by a short drier period between March and April. The station receives approximately 3,000 mm of rainfall annually  
141 (mean annual precipitation from 2004 to 2014: 3,102 mm) and has a mean annual temperature of 25.7°C.

142

143 The core area of the Paracou research station (approximately 500 ha) is predominantly covered by lowland terra firme  
144 rainforest. This old-growth forest has experienced no major human disturbance, although there are signs of pre-Columbian  
145 activities. Species richness is high, with more than 750 woody species recorded, and 150 - 200 tree species per hectare with  
146 DBH above 10 cm. A few dominant botanical families characterise the vegetation: Fabaceae, Chrysobalanaceae,  
147 Lecythidaceae, Sapotaceae, and Burseraceae. The local heterogeneity of the floristic composition is mainly driven by soil  
148 drainage. AGB, measured on trees with a DBH  $\geq$  10 cm, ranges from 286.10 to 450 Mg/ha.

149

150 Following an initial inventory in the early 1980s, 12 permanent 6.25 ha plots were established in 1984. Plot corners, perimeters,  
151 and inner trails (defining four subplots) were verified ~10 years later by a professional land surveyor. Nine plots were logged,  
152 and six received additional silvicultural treatments between 1986 and 1988, creating a disturbance gradient with AGB losses  
153 of 18–25% (treatment 1), 40–52% (treatment 2), and 48–58% (treatment 3). In the early 1990s, three more 6.25 ha plots and  
154 one 25 ha plot were added, totalling ~120 ha of forest censused annually (controls), biennially (disturbed plots), or every five  
155 years (25 ha plot). All 6.25 ha plots are subdivided into four subplots (see Fig. 1), with relative tree coordinates recorded. Trees  
156 and palms  $\geq$  10 cm DBH are mapped, identified, tagged, and periodically measured, forming a database of >70,000 trees. Since  
157 2003, a 57 m flux tower has measured greenhouse gas fluxes, and an N, P, NP fertilisation experiment has been ongoing since  
158 2015.

Deleted: 1

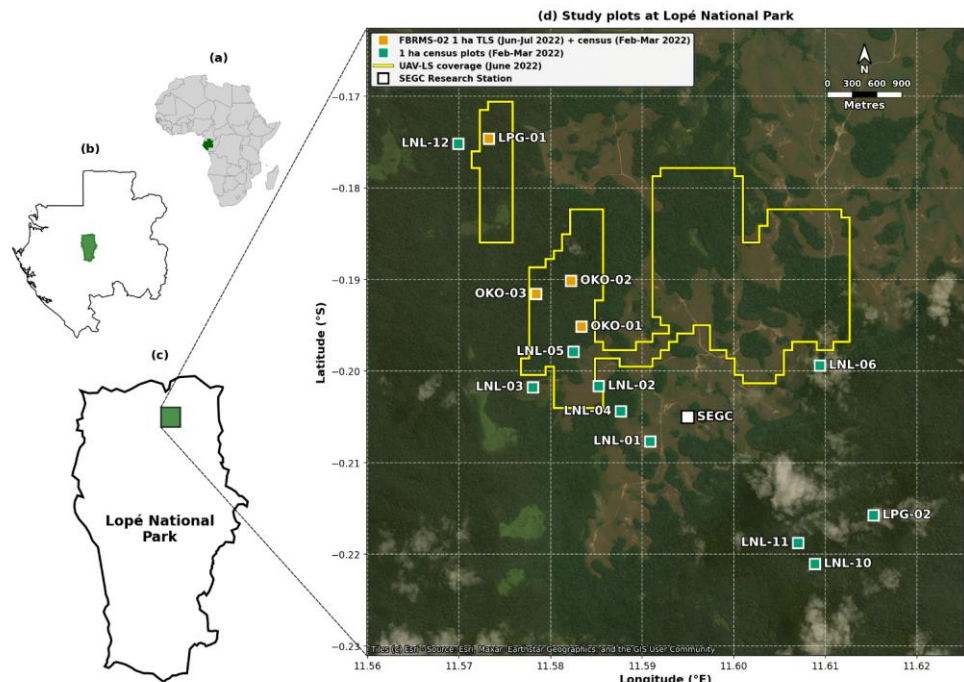
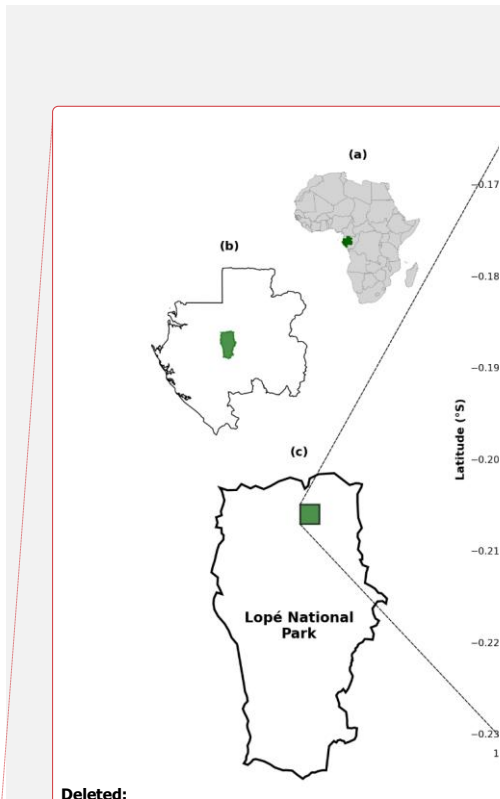


Figure 2: Multi-scale map showing the location and spatial distribution of research plots within Lopé National Park, Gabon. (a) Location of Gabon (green) within Africa. (b) Location of Lopé National Park (green) within Gabon. (c) Park boundary showing the research site location (green). (d) Detailed site map showing the spatial distribution of 14 one-hectare research plots. The four ForestScan FBRMS-02 plots (LPG-01, OKO-01, OKO-02, OKO-03; orange squares) were scanned using TLS during Jun-Jul 2022 with tree census data collected during Feb-Mar 2022. Tree census data was also collected for another ten plots (green circles) which are not part of the ForestScan project. Yellow outlined areas indicate coverage of UAV-LS conducted in Jun 2022. The SEGC (Station d'Études des Gorilles et Chimpanzés) research station is marked with a white square. Map data: Natural Earth 10m cultural vectors. Satellite imagery basemap: Esri World Imagery (Esri, Maxar, Earthstar Geographics, and the GIS User Community). Map projection: WGS84 (EPSG:4326).

Lopé National Park is a 5000 km<sup>2</sup> protected area in central Gabon (Latitude 0°30'S and Longitude 11°30'E), comprising predominantly intact old-growth moist tropical forest. The northern part of the park



Deleted: Orange shaded

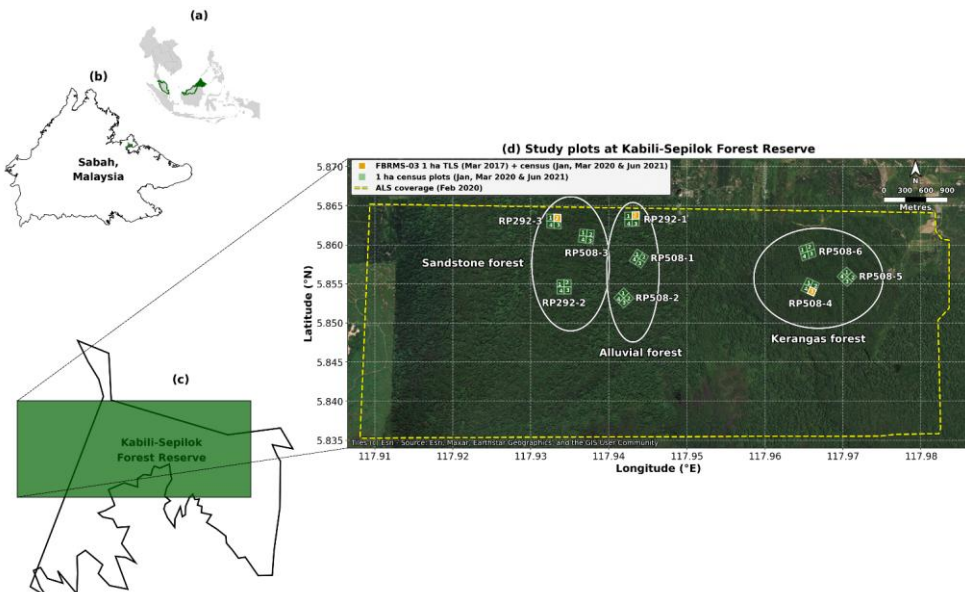
Deleted: yellow

177 features a savanna-forest mosaic, an anthropogenically maintained remnant of the landscape from the Last Glacial Maximum.  
178 The broader landscape is designated as a UNESCO World Heritage Site.

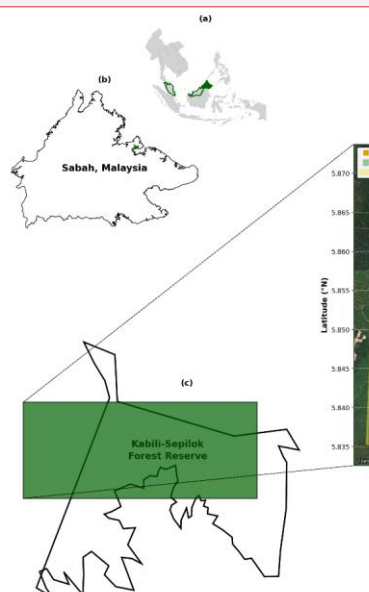
179  
180 The transition from savanna to old-growth forest in the northern part of the park is characterised by six distinct forest types  
181 (Cuni-Sanchez et al., 2016; White et al., 1995): (i) savanna, (ii) colonising forest, (iii) monodominant Okoume forest, (iv)  
182 young Marantaceae forest, (v) mixed Marantaceae forest, and (vi) old-growth forest.

183  
184 A substantial and varied body of literature has emerged from research conducted in Lopé National Park (Agence Nationale  
185 Des Parcs Nationaux, 2025). More than 100 long-term censused forest plots have been established within the park, contributing  
186 significant ground data for the calibration and validation of EO instruments (i.e. Duncanson et al., 2022; Saatchi et al., 2019).  
187 These plots also support various other research activities, such as the Global Ecosystem Monitoring (GEM) Network, an  
188 initiative aimed at understanding forest ecosystem functions and traits (Malhi et al., 2021).

189 **BRMS-03: Kabili-Sepilok, Malaysian Borneo**



Deleted: F



Deleted:

193 **Figure 3:** Multi-scale map showing the location and spatial distribution of research plots at Kabilis-Sepilok Forest Reserve,  
194 Sabah, Malaysian Borneo. (a) Location of Sabah (green) within Malaysia (green boundary) in Southeast Asia. (b) Location  
195 of the Kabilis-Sepilok Forest Reserve (green) within Sabah. (c) Kabilis-Sepilok Forest Reserve area and site map area of panel  
196 d (green rectangle). (d) Detailed site map showing the spatial distribution of 9 x 4 ha plots (labelled RP291-1, RP292-3, etc.)  
197 each containing four 1 ha subplots numbered 1 - 4 (36 subplots in total; green polygons with white subplot numbers) across  
198 three soil types: Alluvial forest, Sandstone forest, and Kerangas forest (delineated by black ellipses). The three FBRMS  
199 subplots are SEP-11 (subplot 2 of plot RP292-3, sandstone soil), SEP-12 (subplot 2 of plot RP292-1, alluvial soil) and SEP-  
200 30 (subplot 3 of plot RP508-4, kerangas soil). Three ForestScan FBRMS-03 1 ha subplots (orange ~~squares~~) were scanned  
201 using TLS during March 2017 and tree census for all subplots was collected in Jan, Mar of 2020 and Jun 2021. Yellow ~~based~~  
202 ~~outline~~ indicates ALS coverage acquired in February 2020. Scale bar: 1000 m. Map data: Natural Earth 10m cultural vectors.  
203 Satellite imagery basemap: Tiles ©Esri - Source: Esri, Maxar, Earthstar Geographics, and the GIS User Community. Map  
204 projection: WGS84 (EPSG:4326).

205 The Kabilis-Sepilok Forest Reserve is located on the Sandakan Peninsula in North-East Sabah, Malaysia, and encompasses  
206 approximately 4,300 hectares of intact old-growth tropical forest. Sepilok has been protected since its establishment by the  
207 Sabah Forest Department in 1931. The elevation ranges from 50 to 250 metres above sea level. This topographic variation,  
208 combined with edaphic differences, results in three distinct forest types: (i) lowland mixed dipterocarp forest overlaying  
209 alluvial soil in the valleys, (ii) sandstone hill forest on hillsides and crests, and (iii) lowland mixed dipterocarp and kerangas  
210 forest at higher elevations (Sabah Forestry Department, n.d.).

211  
212 Between 1995 and 2000, the Ecology Section of the Sabah Forestry Department established 36 one-hectare censused forest  
213 stands across these forest types, as illustrated in Fig. 3.

## 214 **2.2 Data**

### 215 **2.2.1 Tree census**

216 Quality-controlled, tree-by-tree data on identity (tag number and species) and diameter size for all sampled plots in each of the  
217 three FBRMS were collected using global standard tropical forest plot inventory protocols (Forestplots.Net et al., 2021). This  
218 ensured a consistent, full species-level census for all plot trees with a diameter equal to or greater than 10 cm at each FBRMS.  
219 Censuses provide tree-by-tree records that can potentially be linked to laser-scanning approaches. Species identity plays a key  
220 role in determining tree biomass through its strong influence on wood density. While laser-scanning techniques provide  
221 excellent measurements of tree dimensions (such as height and volume), they still require wood density estimates to convert  
222 these volumes into accurate biomass values (see Goodman et al., 2014). Census data also provide tree-by-tree measurements  
223 of tree diameter and whole forest basal area. Finally, because they are independent of constantly changing sensor technologies,  
224 when sustained over time, the core measurement protocols in forest plots deliver long-term consistency for tracking forest  
225 biomass change, growth, mortality, demography, and their trends over decades.

**Deleted:** polygons

**Deleted:** shading

229 Census data for FBRMS plots in Gabon and Malaysia are available via ForestPlots.net (<https://forestplots.net/>, Forestplots.Net  
230 et al., 2021; Lopez-Gonzalez et al., 2011). ForestPlots.net is an internet-based facility with functionality to support all aspects  
231 of forest plot data management, including archiving, quality control, sharing, analysis, and data publishing via stable URLs  
232 (DOIs). ForestPlots.net currently supports the data management needs of more than 2,000 contributors working with 7,000  
233 plots across 23 participating tropical networks. Data access requires potential users to provide details of their planned use and  
234 agreement to abide by requirements for the inclusion of all contributing researchers. This encourages maximum inclusivity of  
235 data originators and is recognised as a key part of what is required to maintain long-term investment in people and infrastructure  
236 that enables continued measurements in these areas (De Lima et al., 2022).

237 **Tree census: FBRMS-01: Paracou, French Guiana**

238 In the Paracou FBRMS, tree censuses are conducted by two teams of three to five permanent field staff using Qfield on field  
239 tablets (since 2020, field computers were used prior to this). Tree girth is measured with a measuring tape at 1.3 m, except  
240 when buttresses necessitate a higher measurement point. The point of measurement (POM) is marked with paint to ensure the  
241 exact same point of measurement between censuses. POM and its potential changes are recorded. New recruits -trees that have  
242 grown beyond 10 cm DBH since the previous survey- are recorded by the field team using vernacular names, and their positions  
243 are measured relative to the original trees. To ensure accurate identification, periodic botanical campaigns are conducted by  
244 one or two experienced botanists, who also correct any misidentifications. When species cannot be identified in the field,  
245 samples are collected and examined at the EcoFoG herbarium in Kourou or the IRD herbarium in Cayenne. All identifications  
246 follow the Angiosperm Phylogeny Group (APG) IV plant classification system. Dead trees and the cause of their death are  
247 recorded. Data are checked for errors after field census using an R script. Any abnormal measurement (e.g., girth showing  
248 abnormal increase/decrease, missing value) is then rechecked in the field in the weeks following the initial census.

249  
250 Plot descriptions for the Paracou FBRMS plots FG5c1, FG6c2 and FG8c4 are accessible via the Guyafor DataVerse  
251 (<https://dataVERSE.cirad.fr>). This internet-based data repository provides plot descriptions and datasets downloadable as CSV  
252 files, together with the corresponding metadata (Derroire et al., 2023). The ForestScan Project data package, including the  
253 latest tree census data used in our analysis and collected in August 2023 for FBRMS plot FG5c1, in June 2023 for plot FG6c2,  
254 and in September 2023 for plot FG8c4, is accessible via  
255 <https://dataVERSE.cirad.fr/dataset.xhtml?persistentId=doi:10.18167/DVN1/94XHID> (Derroire et al., 2025).

256 **Tree census: FBRMS-02: Lopé, Gabon**

257 In the Lopé FBRMS, tree census data was collected at 12 plots in 2017 for the ESA AfriSAR campaign. During June - July  
258 2022, these 13 plots plus one additional 1 ha plot (LPG-02) were re-censused, making a total of 11 x 1 ha forest plots, plus 3  
259 x 1 ha plots in savanna (see Fig. 2). The 10 ha plots included LPG-01, OKO-01, OKO-02 and OKO-03, the 4 x 1 ha FBRMS  
260 plots where TLS was conducted in 2017 and 2022.

261 **Tree census: FBRMS-03: Kabihi-Sepilok, Malaysian Borneo**

262 In the Kabihi-Sepilok FBRMS, tree census data was collected during 2020 - 2022 for a total of 9 x 4 ha plots (IDs RP291-1,  
263 RP292-3, etc. see Fig. 3) each containing four 1 ha subplots numbered 1 – 4 and covering most of the long-term plots at this  
264 site. The three FBRMS subplots SEP-11 (subplot 2 of plot RP292-3, sandstone soil), SEP-12 (subplot 2 of plot RP292-1,  
265 alluvial soil) and SEP-30 (subplot 3 of plot RP508-4, kerangas soil) were scanned using TLS during March 2017 and tree  
266 census for all subplots was collected in Jan, Mar of 2020 and Jun 2021. The 2020-2022 census was overdue as these plots had  
267 not been censused since 2013.

268

269 Plot meta-data, including geography, institution, personnel and historical context, as well as tree-level census attributes (tag,  
270 identity, diameter, point of measurement, stem condition, height, sub-plot, and, where measured x, y coordinates of 5 x 5 m  
271 subplots) and multi-census attributes (tree demography and measurement trajectory and protocols, including growth, point of  
272 measurement changes, recruitment, mortality, and mortality mode) were recorded for all Gabonese and Malaysian FBRMS  
273 plots.

274

275 The ForestScan Project data package, includes data from the 2022 tree census collected during February and March for the  
276 Gabon FBRMS plots and the Malaysian FBRMS plots census data collected in October 2020 for FBRMS plot SEP-11, in  
277 March 2020 for plot SEP-12, and in June 2021 for plot SEP-30. This data package can be accessed via  
278 [https://doi.org/10.5521/forestplots.net/2025\\_2](https://doi.org/10.5521/forestplots.net/2025_2) (Chavana-Bryant et al., 2025).

279 **2.2.2 Terrestrial Laser Scanning (TLS)**

280 TLS data was collected to provide state-of-the-art estimates of tree- and stand-scale AGB for each FBRMS. These LiDAR  
281 measurements, collected using the protocol described in the following sections, produce 3D point clouds with millimetre-level  
282 accuracy representing the forest at each FBRMS. TLS chain sampling protocols (Wilkes et al., 2017), as illustrated and  
283 described in Fig. 4, were employed at all three FBRMS. This data was processed to construct explicit Quantitative Structural  
284 Models (QSMs) describing individual trees within each FBRMS with a DBH  $\geq$  10 cm. Tree- and stand-scale AGB estimates  
285 were then calculated from the volumes of these models, using wood density values derived from published sources based on  
286 species identification from botanical surveys.

287

288

289

290

291

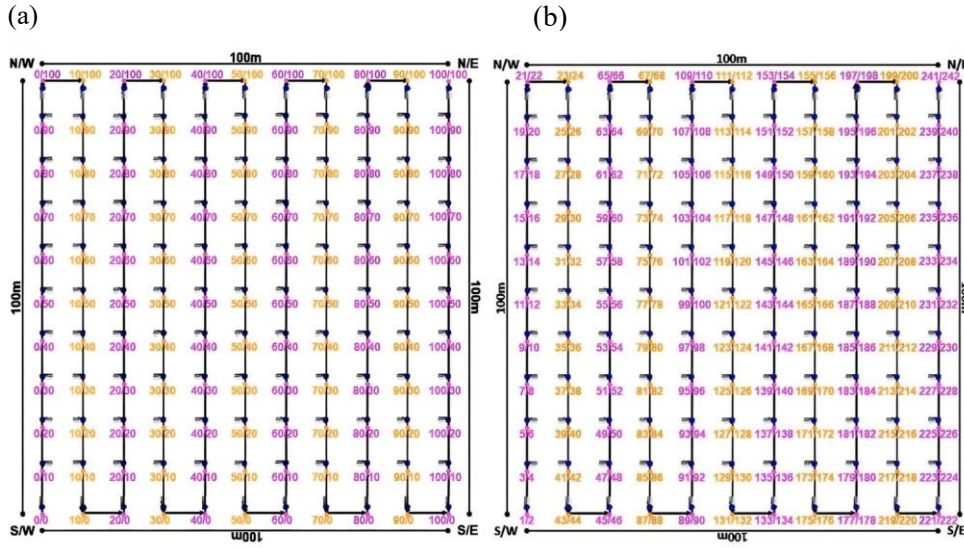
292

Deleted: ¶

300  
301

**Figure 4:** TLS chain sampling was employed to capture high-quality LiDAR data suitable for accurate tree- and stand-scale AGB estimation. Chain sampling was deployed over a 10 m Cartesian grid, resulting in 11 sampling lines with 11 scan positions along each line (i.e., 0 – 10) within 1 ha forest plots. Sampling lines were established in a south-to-north direction (standard practice) and colour-coded using flagging tape, with the ID of each scan position written in permanent marker. Scan positions were identified by their line number and grid position, as shown in panel b (left). Due to the scanner's 100° field of view, capturing a complete scene at each scan position required two scans—upright and tilted. Consequently, 242 scans were collected from 121 positions at each 1 ha forest plot. The order in which the 242 individual scans were collected at each plot is depicted in panel b (right). The first scan at each plot was collected at the southwest corner, i.e., scan position 0,0 (unless impeded by obstacles such as streams, large tree falls, etc., or if the plot was oriented differently). To facilitate scan registration, all tilt scans along the first sampling line were oriented towards the same sampling position along the next sampling line, and all other tilt scans along plot edges were oriented towards the inside of the plot so that the previous scan location was within the tilt-scan field of view. Depending on the density of the canopy understory, terrain, and wind conditions (ideally, low to zero wind and no rain or mist/fog), a team of three experienced TLS operators required 1–2 full working days (8 hrs per day) to set up the chain sampling grid and 3–5 full days to complete the scanning of a 1 ha plot.

315  
316 TLS data for all three FBRMS were collected using a RIEGL VZ-400 laser scanner or its newer model, the VZ-400i, which  
317 has very similar technical specifications (see Table 1) and includes Global Navigation Satellite System (GNSS) Real-Time



318 Kinematic (RTK) positioning (RIEGL Laser Measurement Systems GmbH, 2025). RTK GNSS facilitates TLS data acquisition  
 319 by replacing the labour-intensive and time-consuming task of placing and continuously relocating retro-reflective targets  
 320 between scan positions as required by the RIEGL VZ-400 scanner. Common targets between adjacent scan locations were  
 321 later identified and used to create a registration chain that integrates the 3D point cloud of a scanned plot. GNSS RTK has  
 322 replaced the use of common targets, enabling the absolute (latitude, longitude, and altitude) and relative (between base and  
 323 rover GNSS) positioning of individual scans with centimetre precision, which makes the auto-registration of scans in real-time  
 324 possible. This GNSS-enabled auto-registration significantly reduces the time and effort required to both collect and register  
 325 TLS data. Furthermore, data collected with the VZ-400i are backwards compatible with data from the older VZ-400 scanner,  
 326 allowing for consistent processing and comparison over time.

327

328 **Table 1:** RIEGL laser scanners (RIEGL Laser Measurement Systems GmbH, 2025) ~~and user-defined characteristics~~ for TLS  
 329 data acquisition at ForestScan FBRMS.

Characteristic	RIEGL VZ-400	RIEGL VZ-400i
Wavelength [nm]	<del>~1550 (near-infrared)</del>	<del>~1550 (near-infrared)</del>
Ranging accuracy / precision [mm]	<del>5 / 3</del>	<del>5 / 3</del>
Max range [m]	<del>~800 @ 80% reflectivity</del>	<del>~800 @ 80% reflectivity</del>
Beam divergence [mrad]	<del>0.35</del>	<del>0.35</del>
Beam diameter at emission [mm]	<del>7</del>	<del>7</del>
Returns per pulse	<del>Up to 7</del>	<del>Unlimited (waveform)</del>
GNSS RTK positioning	<del>No</del>	<del>Yes (integrated)</del>
Max Pulse Repetition Rate [kHz]	300 – 1200 (300 used)	300 – 1200 (300 used)
Angular resolution	<del>0.04° with 22.4 million emitted pulses per scan (5.42 billion per hectare)</del>	<del>0.04° with 22.4 million emitted pulses per scan (5.42 billion per hectare)</del>
FOV [°]	<del>360 (horizontal) 100 (vertical)</del>	<del>360 (horizontal) 100 (vertical)</del>
Scan time per scan	3 minutes	3 minutes
Weight [kg]	<del>~13</del>	<del>~13</del>
Operated by	UCL	UCL
Scan site (s)	FBRMS-03: Malaysia	FBRMS-01: French Guiana FBRMS-01: Gabon

**Deleted:** Characteristics of

**Deleted:** used

**Deleted:** E

**Deleted:** I

**Formatted Table**

**Deleted:** (

**Deleted:** , i.e.

**Deleted:** Wavelength [nm]

**Deleted:** Ranging accuracy / precision [mm]

**Deleted:** GNSS RTK positioning

339

340 **TLS: FBRMS-01: Paracou, French Guiana**

341 TLS data was collected in Paracou over two separate periods due to interruptions caused by the COVID-19 pandemic. The  
 342 first campaign took place in 2019, censused plot FG6c2 was scanned with a RIEGL VZ-400 scanner during October and  
 343 November (Brede et al., 2022a). The scanning was conducted over a 200 x 200 m<sup>2</sup> area (i.e. two 1 ha plots) covering two of  
 344 plot 6 subplots -2 and 4- (see Panel c in Fig. 1), resulting in 21 x 21 scan lines with 10 m grid spacing. Retro-reflective targets  
 345 were placed between scan positions to facilitate coarse registration (Wilkes et al., 2017).

346

347 The second TLS campaign took place in 2022, three 1 ha censused plots (see Fig. 1) were scanned during September and  
 348 October using a RIEGL VZ-400i scanner with GNSS RTK-enabled auto-registration. These plots were selected to represent  
 349 the disturbance gradient found at this site, as shown in Table 2. All three plots were also scanned with ALS and plot FG6c2  
 350 additionally scanned with UAV-LS.

351

352 **Table 2:** Overview of plots scanned in 2022 with TLS in Paracou, French Guiana. [We provide both ForestScan plot IDs and](#)  
 353 [their corresponding census plot and subplot IDs used by the census internet-based data repositories.](#)

Plot ID	Census Plot / Subplot ID	Logging treatment	Description	AGB	Lat	Long
FG6c2	<a href="#">6 / 2</a>	Control	Old-growth, lowland, Terra firme rainforest	High	5.27	-52.92
FG5c1	<a href="#">5 / 1</a>	T2	Old-growth, lowland, Terra firme rainforest with mid-level logging disturbance	Mid	5.27	-52.92
FG8c4	<a href="#">8 / 4</a>	T3	Old-growth, lowland, Terra firme rainforest with high-level of logging disturbance	Low	5.26	-52.93

\* Formatted Table

354

355 **TLS: FBRMS-02: Lopé, Gabon**

356 TLS data was collected in 2022, four 1 ha plots were scanned using a RIEGL VZ-400i with GNSS RTK-enabled auto-  
 357 registration, eliminating the need for retro-reflective targets between scan positions. The four sampled plots, shown in Table  
 358 3, were selected to represent the diversity of forest types found within this site.

359

360 **Table 3:** Overview of plots scanned with TLS in Lopé National Park, Gabon. [We provide both the ForestScan plot IDs and](#)  
 361 [their corresponding census plot and subplot IDs used by the census internet-based data repositories.](#)

Plot ID	Census Plot ID	Description	Lat	Long
OKO-01	LNL-07	Maturing secondary Okoumé forest	-0.19	11.58
OKO-02	LNL-08	Maturing secondary Okoumé-Sacoglottis forest	-0.19	11.58
OKO-03	LNL-09	Maturing secondary Okoumé forest	-0.19	11.57
LPG-01	LPG-01	Old-growth forest	-0.17	11.57

**Deleted:** (local plot name / forest type)  
**Formatted Table**  
**Deleted:** LNL-07  
**Deleted:** OKO-01 /  
**Deleted:** LNL-08  
**Deleted:** OKO-02 /  
**Deleted:** LNL-09  
**Deleted:** OKO-03 /  
**Deleted:** Angak /

362

### 363 TLS: FBRMS-03: Kabili-Sepilok, Malaysian Borneo

364 TLS data was collected for three 1 ha forest plots at this FBRMS during March 2017. The three sampled plots, shown in Table  
 365 4, were selected to represent the three distinct forest types found within this site. A RIEGL VZ-400 scanner was used, with  
 366 retro-reflective targets positioned between scan locations to facilitate coarse registration (Wilkes et al., 2017).

367

368 **Table 4:** Overview of plots scanned with TLS in Kabili-Sepilok Forest Reserve, Malaysia. We provide both the ForestScan  
 369 plot IDs and their corresponding census plot and subplot IDs used by the census internet-based data repositories.

Plot ID	Census Plot / Subplot ID	Description	Lat	Long
SEP-11	RP292-3 / 2	Sandstone forest	5.86	117.94
SEP-12	RP292-1 / 2	Alluvial forest	5.86	117.93
SEP-30	RP508-4 / 3	Kerangas forest	5.86	117.97

**Deleted:** Note: subplot 2 was  
**Deleted:** (local plot name / forest type)  
**Formatted Table**  
**Deleted:** 292/3 /  
**Deleted:** 292/1 /  
**Deleted:** 508/4 /

370

### 371 TLS data processing

372 TLS data was collected and processed to provide state-of-the-art estimates of tree- and plot-scale structural attributes and AGB  
 373 for each ForestScan FBRMS. Five main processing steps are required to retrieve structural attributes from the acquired TLS  
 374 data are described below. These processing steps demand significant computational resources -a full 1 ha plot can take 3.4 to  
 375 4 days to process from start to finish on a high performance computing (HPC) cluster, running on multiple central processing  
 376 units (CPUs; general-purpose processors optimised for sequential tasks and complex logic) and graphics processing units  
 377 (GPUs; highly parallel processors ideal for deep learning, point cloud processing and simulations tasks that can be broken into  
 378 thousands of simultaneous operations).

379

393 **1. Individual scan registration into plot-level point cloud**

394 This process was carried out using retro-reflective targets positioned between scan locations to facilitate coarse registration for  
395 data collected with the RIEGL VZ-400 or in a near-automated manner using the RIEGL VZ-400i's GNSS RTK positioning  
396 capabilities in conjunction with the enhanced RIEGL RiSCAN Pro software (versions 2.14–2.17). The integrated Auto  
397 Registration 2 (AR2) function employs GNSS RTK data to update the scanner's position and orientation, including in tilt  
398 mode, thereby enabling real-time automated coarse registration during scanning without the use of retro-reflective targets.  
399 Major registration errors are easily detected, typically occurring during pre-processing in RiSCAN Pro when individual scans  
400 fail to register (i.e., no coherent solution is found) or are incorrectly positioned, which is visually apparent. In cases where  
401 coarse registration/auto-registration fails, unregistered scans can be identified, adjusted, and refined using Multi Station  
402 Adjustment 2 (MSA2), which is also used for final precise registration of data initially coarse-registered using retro-reflective  
403 targets. The registered plot point cloud is provided in the project's local coordinate system. Following this workflow, the co-  
404 registration of all TLS point clouds achieves sub-centimetre accuracy, as confirmed through post-registration inspection. Wind  
405 and occlusion are key sources of uncertainty for the scan registration process, highlighting the necessity of scanning under low  
406 or zero wind conditions and capturing both tilt and upright scans at each location.

407  
408 The use of GNSS significantly enhances the utility and accessibility of TLS by drastically reducing both data acquisition and  
409 processing time. This is achieved by (1) as previously mentioned, replacing the previous labour-intensive and time-consuming  
410 practice of using common retro-reflective targets to link adjacent scan positions into a registration chain (Wilkes et al., 2017),  
411 and (2) reducing the manual processing registration time by an experienced user to 1 - 2 days per hectare, which is less than  
412 half the time required when using retro-reflective targets.

413  
414 Registration results in a plot-level point cloud, comprising 242 individual scan-level point clouds, potentially containing more  
415 than 5.42 billion points.

416  
417 The subsequent four processing steps were performed in a semi-automated manner using the *rxp-pipeline* (Wilkes and Yang,  
418 2025a) and *TLS2trees* processing pipelines (Wilkes et al., 2023) and *TreeQSM* version 2.3 (Raumonen et al., 2013), as  
419 described below.

420 **2. Pre-processing of plot-level point clouds**

421 Pre-processing is carried out in three steps using the open-source tool *rxp-pipeline* (Wilkes and Yang, 2025a), which operates  
422 directly on the raw RIEGL scan data. First, the co-registered RIEGL point clouds are filtered to remove points with a deviation  
423 greater than 15 and reflectance outside the range [-20, 5]. The data are then clipped to the plot extent with an additional 20 m  
424 buffer around the plot, segmented into 10 m x 10 m tiles, and converted from the RIEGL proprietary .rxp to .ply format to

**Formatted:** Font: (Default) +Headings (Times New Roman)

**Formatted:** Font: (Default) +Headings (Times New Roman),  
Not Bold

**Formatted:** Font: Not Bold

**Formatted:** Font: (Default) +Headings (Times New Roman),  
Not Bold

**Formatted:** Font: (Default) +Headings (Times New Roman)

**Formatted:** Font: (Default) +Headings (Times New Roman),  
Not Bold

**Formatted:** Font: (Default) +Headings (Times New Roman)

426 enable further processing. Second, to reduce computing load, the tiled point clouds are downsampled using a voxelisation  
427 approach with a voxel size of 0.02 m, implemented via *PDAL VoxelCenterNearestNeighbor* filter (PDAL Contributors, 2025).  
428 Finally, a tile index mapping the spatial location of each tile is generated. In a HPC system, preprocessing of a 1 ha plot can  
429 take 1.58 to 4.17 hours to complete.

430 **3. Semantic segmentation: wood-leaf separation**

431 *TLS2trees* is an open-source Python command-line pipeline (Wilkes et al., 2025) designed to automate tree extraction from  
432 TLS point clouds by utilising GPUs for parallel computation, making it fully scalable on HPC systems (Wilkes et al., 2023).  
433 The first of the two-step *TLS2trees* workflow employs a deep-learning based approach, implementing a modified version of  
434 the Forest Structural Complexity Tool (FSCT) deep learning semantic segmentation method by Krisanski et al. (2021) to  
435 classify points within tiled point clouds into homogeneous classes representing distinct biophysical components: leaf, wood,  
436 coarse woody debris, or ground. An example of the wood and leaf classes extracted from tree-level point clouds is illustrated  
437 in Fig. 5. In a HPC system, semantic segmentation of a 1 ha plot can take 4 to 12 hours to complete.

438  
439 A comparison of the leaf-wood separation between *TLS2trees* and manual labelling showed a Jaccard index of between 54 -  
440 87% across varying tropical sites (Wilkes et al., 2023). A number of TLS leaf-wood separation approaches have been  
441 developed, using deep learning, or geometric approaches. Unsurprisingly, they all tend to perform worse for taller trees, higher  
442 in the canopy (Arrizza et al., 2024). In *TLS2trees*, the impact of misclassifying (or missing) leaves, is to truncate smaller  
443 branches (Wilkes et al., 2023), reducing the contribution to volume (and hence biomass). This tends to have less impact on tall  
444 tropical trees, than on smaller more dense crowns of deciduous woodland (Calders et al., 2022).



446  
447 **Figure 5:** Tree-level point cloud of the largest *Baillonella toxisperma* (Maobi) tree (~40 m tall with an almost circular

Formatted: Font: Italic

Formatted: Font: Italic

448 canopy ~50 m wide) in plot LPG-01, FBRMS-02: Lopé, Gabon. Points are classified and displayed by category only: wood  
449 points in brown and leaf points in green.

450 **4. Instance segmentation: individual tree separation**

451 The second step in the *TLS2trees* workflow identifies and segments individual trees via a 2-step process. The Dijkstra's shortest  
452 path method first groups all points identified as wood into a set of individual woody stems to which points identified as leaf  
453 are then assigned. A small group of trees automatically segmented from a plot in Gabon are shown in Fig. 6. In a HPC system,  
454 instance segmentation of a 1 ha plot can take 15-20 hours to complete.

455



456 **Figure 6:** Individual tree-level point clouds acquired from plot LPG-01 in FBRMS-02: Lopé, Gabon.

457 **5. TreeQSM: quantitative structural models and results**

458 Quantitative structural models (QSMs) were constructed in a near-automated manner from each individually segmented tree  
459 point cloud (woody components only) with a DBH  $\geq 10$  cm within each ForestScan FBRMS plot. This was achieved using the

460 *TreeQSM* software package (version 2.3; Raumonen et al., 2013), which reconstructs underlying woody surfaces by fitting  
461 cylinders, as illustrated in Fig. 7. The QSM fitting process involves three steps: (i) reducing each point cloud to a series of  
462 patches, (ii) analysing the spatial arrangement and neighbour relationships among patches, and (iii) robustly fitting cylinders  
463 to common patches.

464

465 The overall QSM fit is controlled by three parameters, which are iterated into 125 different parameter sets, each generating  
466 five models. This yields a total of 625 candidate models per segmented tree. The optimal model is then selected by minimising  
467 the point-to-cylinder surface distance (Burt et al., 2019; Martin-Ducup et al., 2021). Estimates of morphological and  
468 topological traits such as volume, length, and surface area metrics, along with their mean and standard deviation, are derived  
469 from the five models that share the same parameters as the optimal model. This approach provides an estimate of the  
470 uncertainty associated with the resulting volume (Wilkes et al., 2023). In a HPC system, QSMs for a 1 ha plot can take up to  
471 2 days to complete.

472

473



474

475 **Figure 7:** QSMs derived from individual tree-level point clouds acquired from plot LPG-01 in FBRMS-02: Lopé, Gabon.

476  
477 Uncertainty estimates are reported for each ForestScan FBRMS plot and included alongside the final modelling outputs for  
478 every tree in a ‘tree-attributes.csv’ file, generated at the end of the modelling process. Sources of error in QSM fitting can arise  
479 from data acquisition (e.g., wind, leaf occlusion, understory vegetation) and from assumptions inherent in segmentation and  
480 fitting processes. Wilkes et al. (2017) discuss issues related to data acquisition and methodological choices, while Morhart et  
481 al. (2024) quantify their effects on branch size and volume under controlled conditions. Although these impacts are difficult  
482 to assess without reference (harvest) data, Demol et al. (2022) show that, where TLS and harvest data have been compared,  
483 agreement is generally within a few percent of AGB per tree. The report CVS file also includes tree- and plot-level carbon and  
484 AGB estimates, the latter based on a mean pantropical wood density value of  $0.5 \text{ g cm}^{-3}$  derived from the DRYAD global  
485 database of tropical forest wood density (2009). Plot-level AGB was also estimated using DRYAD-derived regional mean  
486 wood densities and is presented in Table 5.

487  
488 Figures of all individually segmented trees arranged by tree DBH size (largest to smallest DBH) are also generated for each  
489 FBRMS plot, examples of which can be seen in Fig. 8. In a HPC system, tree figure for a 1 ha plot can take ~30 mins to  
490 complete. Figure 9 provides a comparison of the distribution of DBH measurements collected by tree census and TLS methods  
491 at each of the 10 ForestScan FBRMS 1 ha plots.

492 **TLS datasets**

493 The following terrestrial LiDAR-derived products are available for each of the 10 ForestScan FBRMS plots:

494 1. Raw terrestrial LiDAR data from each scan (no filtering was applied in RiSCAN PRO), stored in the RXP data stream  
495 format developed by RIEGL.

496 2. Transformation matrices necessary for rotating and translating the coordinate system of each scan, into the coordinate  
497 system of the first scan. Stored in DAT format.

498 3. Pre-processed terrestrial LiDAR data:

499 a. full-resolution 10m tiled plot point clouds including attributes such as XYZ [coordinates](#), scan position index,  
500 reflectance, deviation, etc. stored in polygon PLY format.

501 b. downsampled 10m tiled plot point clouds including attributes such as XYZ [coordinates](#), scan position index,  
502 reflectance, deviation, etc. stored in polygon PLY format.

503 c. A tile\_index file (maps the spatial location of the tiled point clouds) stored in DAT format.

504 d. Bounding geometry files setting plot boundaries with and without a buffer surrounding the plot. Stored in  
505 shapefile SHP, DBF, SHX and CPG formats.

506 4. Downsampled 10m tiled plot point clouds segmented into leaf, wood, ground points or coarse woody debris. Stored  
507 in polygon file format PLY format.

508 5. Wood-leaf separated tree-level point clouds including ~~segmentation results and classification probabilities for each~~  
 509 point are stored in polygon PLY format.

510 6. QSM files:

511 a. **in\_plot** CSV (for plots processed with *TLS2trees*) lists all trees to be modelled with QSMs as they are located  
 512 inside the plot boundary.

513 b. **out\_plot** CSV (for plots processed with *TLS2trees*) lists all trees NOT to be modelled as they are located  
 514 outside the plot boundary.

515 c. **plot\_boundary** CSV (for plots processed with *TLS2trees*) shows the location of all in\_plot trees within each  
 516 plot boundary.

517 d. **QSM processing files** (.MAT Matlab).

518 e. **QSMs** derived from each woody tree-level point cloud, (.MAT Matlab).

519 7. We provide pre-processed and segmented terrestrial LiDAR data in PLY format as it supports full 3D object  
 520 representation, including polygons and geometric primitives, in addition to point data. This is essential for storing  
 521 quantitative structure models (QSMs), which go beyond point clouds to describe tree geometry. The PLY format is  
 522 open, widely supported in Python and R, and can be converted to LAS/LAZ when only point data are required.

523 8. Tree-attributes file (.CSV) containing biophysical parameters derived from both the point clouds and QSMs: DBH,  
 524 tree height, tree-level volume and AGB with uncertainty, plot-level AGB and associated uncertainty.

525 9. Figures of all individually segmented trees arranged by tree DBH size (largest to smallest DBH) for each FBRMS  
 526 plot (see Fig. 8) (PNG image format).

527 10. GNSS coordinates (geographical coordinate system: WGS84 Cartesian) for all scan positions stored in KMZ zip-  
 528 compressed format. These files are available for the seven French Guiana and Gabon FBRMS plots.

**Formatted:** Font: Not Bold

530 These TLS ForestScan FBRMS 1 ha plot datasets are freely available via the Centre for Environmental Data Analysis (CEDA)  
 531 with URLs and DOIs provided in section ~~5, and are accompanied by the [ForestScan example directory structure.pdf](#)~~  
 532 ~~document for guidance on dataset organisation~~.

**Deleted:** .

**Formatted:** Font: (Default) Times New Roman

533 QSMs can be converted to PLY format using open-source tools such as *mat2ply* (Wilkes and Yang, 2025b) and then read by  
 534 various tools such as the widely-used free GUI tool CloudCompare (CloudCompare Development Team, 2025;  
 535 <https://www.cloudcompare.org>), via Python using PDAL (PDAL Contributors, 2025; <https://zenodo.org/records/4031609>) or  
 536 ~~Open3D~~ (Open3D Development Team, 2025; [https://www.open3d.org/docs/0.9.0/tutorial/Basic/file\\_io.html#mesh](https://www.open3d.org/docs/0.9.0/tutorial/Basic/file_io.html#mesh)), or via the  
 537 R Geomorph package (Adams et al., 2025; <https://rdrr.io/cran/geomorph/man/read.ply.html>). In the Geomorph R package, the  
 538 function Read mesh data (vertices and faces) from PLY files can be used to read three-dimensional surface data in the form of  
 539 a single PLY file (Polygon File Format; ASCII format, from 3D scanners). Vertices of the surface may then be used to digitise  
 540 three-dimensional points. The surface may also be used as a mesh for visualising 3D deformations. ~~which refer to changes or~~

**Deleted:** d

544 displacements in the geometry of the object compared to a reference state. This is achieved using the warpRefMesh function.

**Deleted:**

545 The function opens the PLY file and plots the mesh, with faces rendered if file contains faces, and coloured if the file contains  
 546 vertex colour. Vertex normals allow better visualisation and more accurate digitising with digit.fixed. The KMZ files  
 547 containing the GNSS scan position coordinates can be uploaded to Google Earth or read into a GIS tool such as QGIS (QGIS  
 548 Development Team, 2025; <https://qgis.org>).

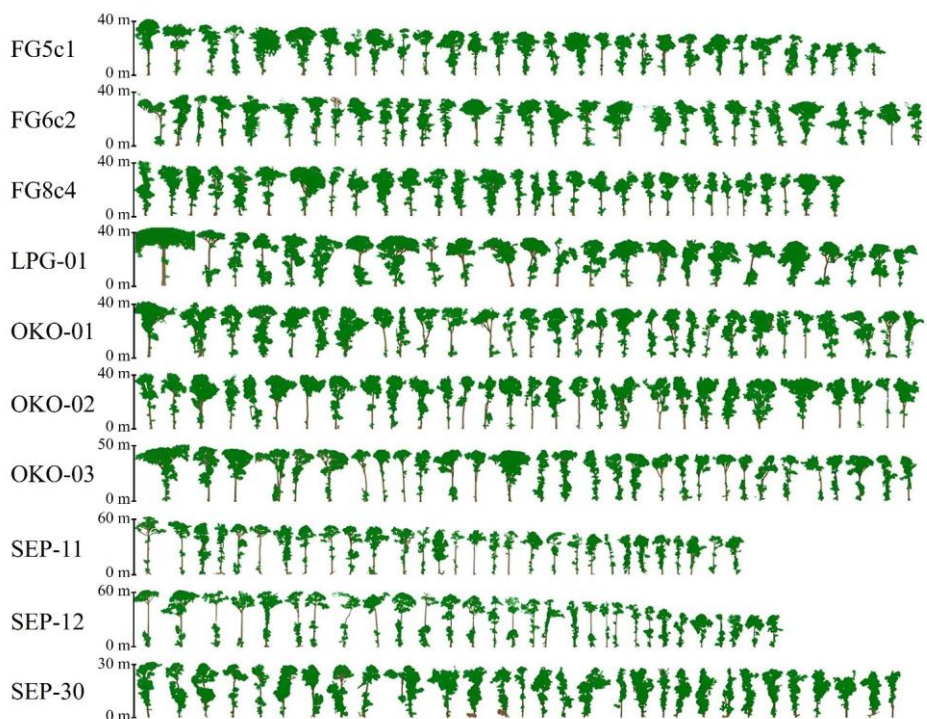
549

550 **Table 5:** Summary statistics for 10 FBRMS ForestScan TLS plot datasets. AGB estimates use wood density values from the  
 551 DRYAD global database (Zanne et al., 2009): (1) *TLS2Trees* pantropical mean, (2) Tropical Africa mean (TAF, Gabon), (3)  
 552 South-East Asia mean (TS-EA, Malaysia), (4) Tropical South America mean (TSA, French Guiana), (5) Guyana community  
 553 mean (GF, French Guiana), and (6) allometric AGB estimates based on Chave et al. (2014).

Plot ID	Site	Cens us trees ( $\geq 10$ cm DB H)	TLS2trees plot summary				TLS2trees Carbon estimation			TLS2trees AGB estimations (1)			Tropical Africa (TAF; 2) / Tropical South America (TSA; 4) / Tropical South-East Asia (TS-EA; 3) AGB estimations			Guyana AGB estimations (5)			2014 Allom etric AGB estima tion (6)	
			TLS trees (#)	TLS vs Census trees (%)	TLS plot area (ha)	TLS plot volum e (m <sup>3</sup> )	Plot C (t)	C per ha (t/ha)	Wood density (g/cm <sup>3</sup> )	Plot AGB (t)	AGB per ha (t/ha)	Wood density (g/cm <sup>3</sup> )	Plot AGB (t)	AGB per ha (t/ha)	Wood density (g/cm <sup>3</sup> )	Plot AGB (t)	AGB per ha (t/ha)	Plot AGB (t)		
OKO-01	GA	388	397	2.58	1.08	829.05	195.24	181.60	0.5	414.52	385.57	0.60	495.77	459.05				378.62		
OKO-02	GA	472	473	0.21	1.02	625.45	147.29	143.97	0.5	312.72	305.67	0.60	374.02	366.69				351.35		
OKO-03	GA	339	355	4.72	1.04	959.59	225.98	218.19	0.5	479.79	463.26	0.60	573.83	551.76				372.82		
LPG-01	GA	340	275	-19.12	1.05	477.88	112.54	107.16	0.5	238.94	227.52	0.60	285.77	272.17				459.85		
FG5c <sub>1</sub>	GF	1110	804	-27.57	1.06	529.67	124.74	117.62	0.5	264.83	249.73	0.63	334.75	315.80	0.73	386.66	409.86	327.30		
FG6c <sub>2</sub>	GF	902	832	-7.76	1.10	751.13	176.89	161.48	0.5	375.57	342.86	0.63	474.72	431.56	0.73	548.33	603.16	421.90		
FG8c <sub>4</sub>	GF	1116	1090	-2.33	1.09	625.80	147.38	135.76	0.5	312.90	288.24	0.63	395.50	362.85	0.73	456.83	497.95	286.10		
SEP-11	MY	584	659	12.84	1.05	961.36	226.40	214.67	0.5	480.68	455.78	0.57	551.82	579.41				499.91		
SEP-12	MY	469	380	-18.99	1.13	765.51	180.28	158.98	0.5	382.76	337.53	0.57	439.40	496.53				443.45		
SEP-30	MY	787	986	25.29	1.03	374.66	88.23	85.25	0.5	187.33	181.01	0.57	215.05	221.50				311.54		

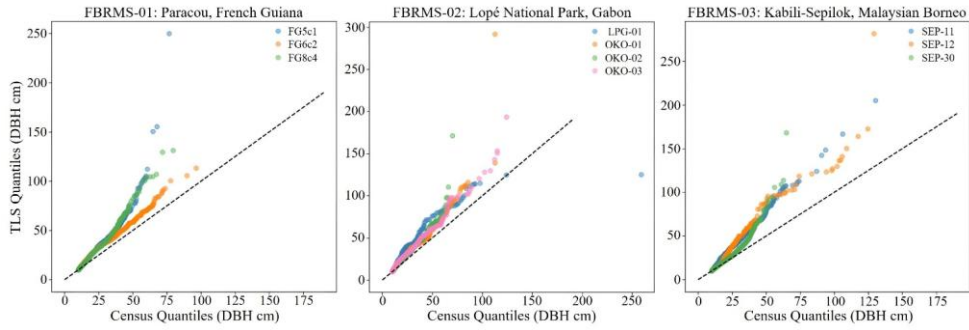
554

556



557

558 **Figure 8:** Examples of the largest trees (up to 30 trees) arranged in decreasing DBH size (1.3 m trunk height) for each of the  
559 10 ForestScan FBRMS plots. The upper limit of the Y axis varies and ranges from 30 m to 60 m maximum tree size between  
560 plots.



561  
562 **Figure 9:** Quantile-Quantile (QQ) plots comparing the distribution of DBH measurements collected by tree census and TLS  
563 methods at each of the 10 ForestScan FBRMS 1 ha plots. TreeQSM measures DBH at the standard height of 1.3 m for each  
564 TLS-extracted tree, whereas census DBH measurements are routinely adapted to account for tree buttresses found among  
565 larger trees. Generally, census and TLS DBH measurements are in good agreement but consistently overestimated by TLS.  
566 Deviations for larger DBH values can be improved by adapting the DBH extraction of large buttressed trees once these trees  
567 are matched to their census counterparts. The 1:1 reference line (dotted black line) represents perfect agreement between  
568 census and TLS-extracted DBH measurements.

569 **2.2.3 Unpiloted Aerial Vehicle laser scanning (UAV-LS)**

570 Unlike TLS, there are currently no best practice guidelines for UAV-LS data acquisition for forest characterisation. Therefore,  
571 flight plans and parameters were implemented on a case-by-case basis, considering the site, instrument, sensor, and application.  
572 An important consideration in this respect is whether VLOS needs to be maintained, i.e., the visibility of the platform by the  
573 pilot throughout the mission. Regulations on this vary nationally and are changing rapidly as technology evolves and the use  
574 of UAVs expands. In Europe, for example, a risk-based approach has been introduced, allowing beyond VLOS when risks are  
575 negligible.

576 Another important consideration is the availability of take-off and landing areas. Vertical take-off and landing (VTOL)  
577 platforms (e.g., quadcopters and octocopters) require smaller areas and are more flexible, while fixed-wing platforms may  
578 require substantial take-off and landing sites, although they offer greater area coverage and flight duration. The actual take-off  
579 area for VTOL platforms is highly dependent on the skills and confidence of the pilot. However, a very small take-off area  
580 surrounded by tree crowns typically also means low chances for VLOS operation, unless an above-canopy platform such as a  
581 cherry-picker is available.

583 In the context of VTOL and VLOS operations, viewshed analysis based on already acquired ALS data has proved useful. ALS  
584 point clouds can be used to derive initial Digital Surface Models (DSM), which can identify possible take-off positions.  
585 Viewshed analysis can then use the DSM to simulate the visibility of the UAV from the take-off position.

587 During data collection, attention should also be paid to acquiring access to GNSS observables from permanent base stations  
588 (e.g., CORS network) or to collecting observables with a temporary base station (e.g., Emlid Reach RS+ or RS2). A base  
589 station should be positioned less than 15 km from the survey area. For some platforms, Real-Time Kinematic (RTK), and  
590 therefore radio connection, between the UAV and base station can be an added constraint.

592 Our UAV-LS data collections used three different LiDAR systems built by RIEGL at FBRMS-01 and FBRMS-02. All systems  
593 are based on the time-of-flight principle and capable of multi-return registration with the miniVUX-1DL being a specific  
594 downward-looking sensor designed for fixed-wing UAVs. Technical specifications for all three UAV-LS sensor systems are  
595 provided in Table 6.

597 **Table 6:** UAV-LS sensor systems used at ForestScan FBRMS-01 and FBRMS-02.

Characteristic	miniVUX-1UAV	VUX-1UAV	miniVUX-1DL
Max Pulse Repetition Rate [kHz]	100	550	100

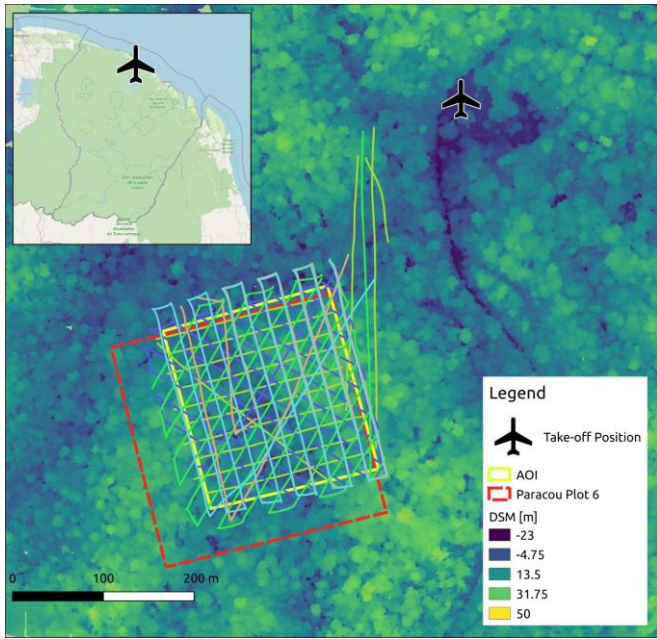
598 Formatted Table

Wavelength [nm]	905	1550	905
FOV [°]	360	330	46
Ranging accuracy / precision [mm]	15 / 10	10 / 5	15 / 10
Max range [m]	330 @ $\rho \geq 80\%$	1050 @ $\rho \geq 80\%$	260 @ $\rho \geq 80\%$
Weight [kg]	1.55	3.5	2.4
Inertial Measurement Unit (IMU)	Applanix APX20	Applanix AP20	Applanix APX15
Operated by	AMAP	Wageningen University	University of Edinburgh
Operated on	DJI M600	RiCOPTER	DELAIR DT26X
Flight location	FBRMS-01: Paracou	FBRMS-01: Paracou	FBRMS-02: Lopé
Flights merged into single acquisition	No	No	Yes

599

600 **UAV-LS: FBRMS-01: Paracou, French Guiana**

601 UAV-LS data was collected in October 2019 using two different scanning systems as shown in Tables 7 and 8. The first set  
 602 of 11 flights listed in Table 7 were conducted using the RIEGL VUX-1UAV mounted on a RIEGL RiCOPTER UAV and  
 603 flown over the same 200 x 200 m<sup>2</sup> area that was scanned with TLS covering subplots 2 and 4 in plot 6. Six of these flights  
 604 covered the entire 200 x 200 m<sup>2</sup> area with 20 m spacing between flight lines at an altitude of 120 m above ground level (AGL).  
 605 The remaining five flights covered only the north-east 100 x 100 m<sup>2</sup> area covering subplot 2 (i.e. FG6c2) with a criss-cross  
 606 pattern to maximise the diversity of viewing angles into the canopy. These latter flights were conducted at a lower altitude of  
 607 90 m AGL to increase point density; however, the entire plot could not be covered without losing VLOS.  
 608



609

610 **Figure 10:** UAV-LS flight trajectories over the FBRMS-01 site at Paracou, showing coverage of the experimental 4 ha plot 6  
 611 (red dashed outline) and the area of interest (AOI; yellow dashed outline). The criss-cross flight pattern results from multiple  
 612 flight lines oriented in different directions (e.g., N–S, E–W, NE–SW) to improve point density and reduce occlusion in dense  
 613 tropical forest canopies. The background shows a digital surface model (DSM) with elevation values (m), colour-coded by  
 614 elevation classes as indicated in the figure legend (–23 m to 50 m). The inset map shows the regional location of Paracou  
 615 within French Guiana (© OpenStreetMap contributors, available at <https://www.openstreetmap.org>).  
 616

617 **Table 7:** Overview of the 2019 VUX-1 UAV-LS flights at FBRMS-01 (Paracou), including [Census Plot ID \(see Table 2\)](#),  
 618 acquisition date/time, flight height above ground level (AGL), speed, and pulse repetition rate. Flight patterns refer to the  
 619 orientation of flight lines: N–S (north–south), E–W (east–west), NE–SW (northeast–southwest), and “criss-cross” indicates  
 620 multiple orientations flown over the same area as seen in Fig. 10. All flights listed can be considered part of one acquisition  
 621 and are provided as individual point clouds in this dataset. Users may merge them according to their needs.

Census Plot ID	Date & Time (UTC ISO 8601)	Direction [°]	Interline [m]	Alt	Speed [ $\text{m s}^{-1}$ ]	Pulse Repetition Rate [kHz]
----------------	----------------------------	---------------	---------------	-----	-----------------------------	-----------------------------

Deleted: p

Formatted: Left

Formatted Table

Deleted: /

				AGL [m]		
6	2019-10-18T11:41:05Z	Manual	20	115	4	550
6	2019-10-18T13:28:27Z	165	20	110	6	550
6	2019-10-18T14:36:54Z	75	20	105	7	550
6	2019-10-18T175:7:53Z	120	20	115	6	550
6	2019-10-18T19:23:14Z	30	20	105	6	550
6	2019-10-19T16:34:12Z	165	20	120	6	300
6	2019-10-20T18:45:40Z	165	20	120	6	100
6	2019-10-19T12:10:41Z	multiple headings	variable	95	4	550
6	2019-10-19T12:41:09Z	multiple headings	variable	85	4	550
6	2019-10-19T18:19:57Z	multiple headings	variable	95	4	550
6	2019-10-19T19:41:42Z	multiple headings	variable	90	4	550

**Deleted:** P

**Deleted:** 200

**Deleted:** P

**Deleted:** 100

**Deleted:** P

**Deleted:** 100

**Deleted:** P

**Deleted:** 100

**Deleted:** P

**Deleted:** 100

624

625 UAV-LS data was also collected over several plots using a different UAV-LS system -a YellowScan Vx20 containing a RIEGL  
626 Mini-VUX scanner and Applanix 20 IMU- mounted on a DJI M600. Details for a second set of 12 flights can be found in  
627 Table 8. To allow for comparisons with the VUX system, coincident acquisitions were performed over experimental plot 6  
628 (covering all four subplots) and several others within the Paracou Research Site (see Table 8).. A full description of the UAV-  
629 LS data collection for this UAV-LS data is provided in Brede et al. (2022b).

630

631 **Table 8:** Overview of UAV-LS flights using a YellowScan Vx20 system (RIEGL Mini-VUX scanner and Applanix 20 IMU)  
632 mounted on a DJI M600 during the 2019 mission at the FBRMS-01 site. Automated flight plans were performed using flight  
633 plans with the UgCS route planning software in grid mode. The table lists plot ID, acquisition date/time, flight parameters  
634 (direction, interline spacing, altitude and speed). Altitude values are reported as specified during flight planning with some  
635 missions using Above Ground Level (AGL), while others used Above Mean Sea Level (AMSL) due to differences in mission  
636 planning and operational requirements. These original specifications are retained to accurately reflect acquisition parameters.  
637 Pulse repetition for the RIEGL Mini-VUX scanner is fixed at 100kHz. Flights cover multiple experimental plots: 4 & 5 (single  
638 flight), 6 (8 flights), 7, 8, 10, 15, and the Tower plot (two flights) within the Paracou Research Site. All listed flights are  
639 provided individually; users may merge flights covering the same plot if needed for analysis.

Census Plot ID	Date & Time (UTC)	Direction [°]	Interline [m]	Alt [m]	Speed [m s <sup>-1</sup> ]	Pulse Repetition Rate [kHz]
4 & 5	2019-10-19T17:23:47Z	345	50	100 amsl	5	100
6	2019-10-18T12:40:06Z	345	20	80 AGL	5	100
6	2019-10-18T13:10:43Z	345	20	80 AGL	5	100
6	2019-10-18T18:30:57Z	120	20	80 AGL	5	100
6	2019-10-18T18:54:16Z	120	20	80 AGL	5	100
6	2019-10-18T20:09:32Z	165	20	145 amsl	5	100
6	2019-10-19T11:59:17Z	75	20	145 amsl	5	100
6	2019-10-19T19:03:45Z	75	20	80 AGL	5	100
6	2019-10-20T19:17:57Z	345	40	100 amsl	3	100
8	2019-10-20T11:39:07Z	75 & 345	50	105 amsl	5	100
GuyaFlux tower/CNES (tropiscat)	2019-10-19T16:25:57Z	0	50	80 AGL	5	100
GuyaFlux tower/CNES (tropiscat)	2019-10-19T18:10:21Z	90	50	105 amsl	5	100

Formatted Table

Deleted: /

Deleted: P

662

### 663 UAV-LS data processing

664 All collected raw data underwent processing with standard tools. For VUX-1UAV data, this included processing  
 665 recorded [global navigation satellite system](#) (GNSS) and base station data to flight trajectories with POSPac [Mobile](#)  
 666 [Mapping](#) Suite 8.3 (Applanix, Richmond Hill, Ontario, Canada), laser waveform processing to discrete returns and geolocation  
 667 in world coordinates with RIEGL RiProcess 1.8.6. For miniVUX-1UAV, waveform processing is performed online in the  
 668 sensor. Point cloud processing and geolocation was performed with the CloudStation software (Yellowscan, Montpellier,  
 669 France), using the Strip Adjustment option. For all UAV-LS data, only points with a reflectance larger than -20 dB were kept  
 670 for further processing. Points with reflectance smaller than -20 dB consist mainly of spurious points caused by water droplets  
 671 under high humidity conditions ([Schneider et al., 2019](#)).

672

687 LiDAR point clouds were processed using the *LASTools* suite (rapidlasso GmbH). First, a 1-m resolution digital surface model  
688 (DSM) was generated with **lasgrid** using the highest return within each cell. Ground points were then classified  
689 with **lasground** (wilderness settings, 15-m step), and a 1-m digital terrain model (DTM) was derived from ground-classified  
690 points using **las2dem**. Heights were normalized by subtracting ground elevation with **lasheight**, producing a set of height-  
691 normalized point clouds. A 1-m canopy height model (CHM) was computed with **lascanopy**, retaining the maximum height  
692 in each grid cell after removing noise and low-confidence classes. Finally, a point density map (1-m resolution) was created  
693 using **lasgrid** with the *counter* option. This workflow produced consistent DSM, DTM, CHM, and density layers suitable for  
694 subsequent ecological analyses. These UAV-LS datasets are [provided in the WGS84 coordinate reference system](#)  
695 [\(EPSG:4326\)](#) and freely available via the Centre for Environmental Data Analysis (CEDA) with DOIs provided in section 5.  
696 Data access.

697 **UAV-LS: FBRMS-02: Lopé, Gabon**

698 UAV-LS data was collected in June 2022, concurrently with TLS data acquisition at this FBRMS. Data was acquired using a  
699 DELAIR DT26X drone platform equipped with a RIEGL miniVUX-1DL (Mcnicol et al., 2021) as seen in Fig. 11. This  
700 platform differs from the one used at FBRMS-01: Paracou in that it is designed for large-scale data acquisitions (thousands of  
701 hectares) and is capable of operating beyond the VLOS, with an average flight speed of  $17 \text{ m s}^{-1}$  ( $61 \text{ km h}^{-1}$ ). Flights were  
702 conducted in perpendicular lines at a nominal altitude of 120 m above the ground surface, with an average flight line spacing  
703 of 20 m (based on 70–80% overlap). Each one-hour flight covered approximately 120–200 hectares with an estimated point  
704 density of 400 points per square metre. To obtain the required densities, several flights were conducted over the core plots  
705 from different angles (depending on wind conditions) to maximise the diversity of viewing angles into the canopy.  
706

Deleted: /

Deleted: /



709

710 **Figure 11:** UAV-LS acquisitions at FBRMS-02: Lopé using a fixed-wing system. This UAV employs a conventional take-off  
 711 and landing (CTOL) procedure, with launch aided by a catapult (top). Once airborne, the UAV is controlled from a laptop  
 712 connected to the UAV via an antenna (middle). The flight trajectory is corrected to centimetre precision using data collected  
 713 from a static GNSS receiver placed within 10 km of the UAV operating area (lower left). Additional refinements and  
 714 corrections are possible via ground control points located across the study area (lower middle), the positions of which are  
 715 measured using a 'rover' GNSS receiver (lower right). Image originally published in McNicol et al. (2021).

716 **UAV-LS data processing**

717 Flight trajectories were reconstructed using GNSS/IMU measurements and adjusted with differentially corrected base station  
718 data in Applanix POSPac software. The corrected flight paths and laser data were then integrated using the RIEGL software  
719 package, RiPROCESS, to generate the initial three-dimensional point cloud. Residual trajectory errors—such as discrepancies  
720 in GPS tracking and elevation—were corrected by using small buildings as reference points to refine the relative position and  
721 orientation of individual flight lines and scans. Further adjustments were made using ground control points: square targets (1–  
722 2 m<sup>2</sup>) composed of alternating black and white material arranged in a checkerboard pattern. Geometric accuracy refers to the  
723 absolute positional accuracy of the final point cloud after these corrections, quantified by the residuals between LiDAR points  
724 and surveyed ground control points. This process resulted in a LiDAR-derived point cloud with a geometric accuracy of 1.8 cm.  
725 All elevation data were calculated as ellipsoidal heights (m) within the UTM 32S coordinate system. Each flight was processed  
726 separately, and all datasets were merged prior to export. Subsequent point cloud processing was carried out using elements of  
727 the lidR package (v3.1.0; Roussel et al., 2020). This UAV-LS dataset is freely available via the Centre for Environmental Data  
728 Analysis (CEDA) with DOIs provided in section 5. Data acquisition characteristics can be found in Table 6.  
729

Formatted: Normal

**Moved down [1]:** Table 9: Comparison of ALS acquisition  
ForestScan sites: FBRMS-01:Paracou, French Guiana and FBRMS-  
03: Kabil-Sepilok, Malaysian Borneo. These key flight and sensor  
characteristics can support alignment and comparability across sites.¶

**Deleted:** ¶

¶ Table 9: Comparison of ALS acquisition characteristics for two  
ForestScan sites: FBRMS-01:Paracou, French Guiana and FBRMS-  
03: Kabil-Sepilok, Malaysian Borneo. These key flight and sensor  
characteristics can support alignment and comparability across sites.¶

**Deleted:** ALS flight characteristics

741 **2.2.4 Airborne Laser Scanning (ALS)**

742 [Table 9](#): Comparison of ALS acquisition characteristics for two ForestScan sites: FBRMS-01:Paracou, French Guiana and  
 743 FBRMS-03: Kabilis-Sepilok, Malaysian Borneo. These key flight and sensor characteristics can support alignment and  
 744 comparability across sites.

<u>ALS flight characteristics</u>	<u>FBRMS-01: Paracou, French Guiana</u>	<u>FBRMS-02: Kabilis-Sepilok, Malaysian Borneo</u>
<u>Date</u>	<u>Nov 2019</u>	<u>Feb 2020</u>
<u>Area covered</u>	<u>10 km<sup>2</sup></u>	<u>27 km<sup>2</sup> (Kabilis-Sepilok) + 20 km<sup>2</sup> (Danum Valley protected area) + 9 km<sup>2</sup> (reduced impact logging area adjacent to Danum Valley)</u>
<u>Scanner</u>	<u>RIEGL LMS - Q780</u>	<u>RIEGL LMS - Q560</u>
<u>Platform</u>	<u>BN2 aircraft</u>	<u>Helicopter</u>
<u>Altitude</u>	<u>~900 m</u>	<u>~350 m (above forest canopy)</u>
<u>Speed</u>	<u>~180 km h<sup>-1</sup> (50 m s<sup>-1</sup>)</u>	<u>~100 km h<sup>-1</sup> (30 m s<sup>-1</sup>)</u>
<u>Scan angle</u>	<u>±30°</u>	<u>±30°</u>
<u>Pulse density</u>	<u>Min 15 pts m<sup>-2</sup>; Mean 40 pts m<sup>-2</sup></u>	<u>Mean 40 pts m<sup>-2</sup></u>
<u>Overlap</u>	<u>80%</u>	<u>40%</u>
<u>CRS</u>	<u>EPSG:2972</u>	<u>EPSG: 32650</u>

**Moved (insertion) [1]**

**Moved (insertion) [2]**

**Formatted Table**

**Deleted:** /

**Deleted:** :

**Deleted:** /

**Deleted:** :

**Deleted:** /

**Deleted:** /

**Deleted:** /

**Formatted:** Normal

745 **FBRMS-01: Paracou, French Guiana**

746 ALS data were acquired over Paracou in November 2019. The data covers 10 km<sup>2</sup>, including all experimental plots and areas  
 747 covered by TLS and UAV-LS (see Fig. 1). During the same campaign, additional data was gathered over Nouragues Research  
 748 Station in French Guiana. This supplementary data was collected using identical scanning characteristics (provided in Table  
 749 9) and has been incorporated into the ForestScan data archive.

750  
 751 ALS data for Paracou are freely available via the Centre for Environmental Data Analysis (CEDA) with DOIs provided in  
 752 section 5. Canopy height models for both Paracou and Sepilok are described in Jackson et al. (2024) and available at  
 753 <https://doi.org/10.908679>.

762 **FBRMS-03: Kabili-Sepilok, Malaysia**

763 ALS data were acquired at Kabili-Sepilok in February 2020. This dataset includes LiDAR and RedGreenBlue (RGB) imagery  
764 data collected from a helicopter over the Kabili-Sepilok Forest Reserve and an additional non-ForestScan site -Danum Valley  
765 Forest Reserve. These areas were selected due to the availability of prior ALS data collected in 2013 and 2014. The complete  
766 collection and processing details for these datasets are detailed in Jackson *et al.* (2024).

767

768 The point cloud data for this FBRMS are available in LAS (LASer) format, as well as RGB data summary rasters in .tif format.  
769 The raster images were processed with LAStools using default parameters. Canopy Height Model (CHM), Digital Surface  
770 Model (DSM), Digital Terrain Model (DTM), and pulse density (pd) data are also included. The RGB data are provided in  
771 .jpg format and organised by flight date. The data was georeferenced using ground control points. This ALS dataset is freely  
772 available via the Centre for Environmental Data Analysis (CEDA) with DOIs provided in section 5.

773 **3. Recommendations for aligning and matching datasets**

774 We provide data that are internally consistent in terms of pre-processing, geo-referencing, and exported in formats compatible  
775 with open-source tools. Any further processing will depend largely on the intended application, such as individual tree analysis  
776 or plot-level studies.

777

778 For TLS data, all point clouds within a single plot are co-registered into one unified point cloud. These are subsequently  
779 processed into individual tree point clouds, to which quantitative structural models (QSMs) are fitted to estimate volume.  
780 Datasets for FBRMS-01 and FBRMS-02 were acquired using a RIEGL VZ-400i equipped with GNSS RTK positioning.  
781 However, as GNSS performance is often compromised beneath dense tropical canopies, positional accuracy for these datasets  
782 should be interpreted with caution.

783

784 UAV-LS and ALS datasets are geo-referenced, ~~with~~ ~~positional accuracy~~ ~~determined by~~ IMU and GNSS measurements. ~~These~~  
785 ~~measurements~~ can introduce errors ~~that~~ ~~manifest~~ as height biases between individual flight lines. Although ~~no such~~  
786 ~~discrepancies were observed~~ in our data, a ~~definitive assessment would require a rigorous comparison with ground control~~  
787 ~~points~~, a step we have not undertaken. These datasets have not been explicitly aligned or matched to one another. Alignment  
788 ~~is possible~~, but requires manual identification of control points ~~within each dataset~~, as noted above, ~~should be undertaken only~~  
789 ~~if necessary for the intended application of the data~~.

790 **3.1 Matching TLS to census data: stem maps**

791 A key step in estimating AGB from tree-level terrestrial laser scanning (TLS) point clouds is the selection of wood density for  
792 converting volume to mass. Wood density represents a significant source of uncertainty in the indirect estimation of AGB,

**Deleted:** in each case, As p  
**Deleted:** depends  
**Deleted:** on the  
**Deleted:** ,  
**Deleted:** which  
**Deleted:** ing  
**Deleted:** we did not  
**Deleted:** such discrepancies  
**Deleted:** rigorous comparison with ground control points would be  
**Deleted:** d to confirm this definitively  
**Deleted:** can be performed  
**Deleted:** ,  
**Deleted:** it  
**Deleted:** and  
**Deleted:** will depend on the intended use of the resulting

808 whether through allometry and census DBH, EO-derived canopy height, TLS-estimated volume, or other methods (Phillips et  
809 al., 2019). If the censused trees in each plot can be matched to their TLS counterparts, literature estimates of species-specific  
810 WD (or field-measured values, if available) can be used. In the absence of such a match, plot-level mean WD values are  
811 employed, as is common in most EO-derived estimates that rely on large-scale allometric models (e.g. Chave et al., 2014).  
812 Research by Momo et al. (2020), Burt et al. (2020), and Demol et al. (2021) has demonstrated that significant bias can occur  
813 in TLS-derived AGB estimates due to within-tree WD variations when literature-derived species average WD values are used.  
814 However, Momo et al. (2020) suggest there is sufficient correlation between vertical gradients and basal WD to allow for  
815 empirical corrections.

816

817 While it is preferable to match TLS trees to census trees, this process is not straightforward and is currently only possible  
818 manually (if at all) after TLS data acquisition and co-registration. Once registered, a slice through the TLS plot-level point  
819 cloud can be generated, enabling the identification of individual trees from their stem profiles. This stem map can be provided  
820 in hard copy or digital format (e.g., high-resolution PDF) to the census team, who can then revisit the plot, moving through it  
821 in the same manner as during the census—starting at the plot’s southeast corner or 0,0 and moving up and down by 10 m  
822 quadrants—annotating the TLS stem map with each tree census ID. This process can be conducted separately or as part of an  
823 existing census but is best performed simultaneously or as soon as possible after TLS collection to minimise changes and  
824 facilitate collaboration between TLS and census teams. Despite success with this approach in some plots (e.g., Gabon 2016),  
825 experience has shown that significant understory, terrain variation, and/or changes and tree falls between census and TLS data  
826 collection (e.g., ~2 years between census and TLS data collection for FBRMS-03 plots, and significant tree falls and changes  
827 due to a storm between census and TLS data collection in FBRMS plot LPG-01 in Gabon) make this process very challenging,  
828 particularly for smaller stems (in the 10-20 cm DBH range).

829 **3.2 Aligning TLS to UAV-LS data (and other spatial data)**

830 Through its accurate global registration via PPK processing, UAV-LS can be regarded as a high-quality geometric reference  
831 for registration. For the purpose of comparison with accurate ALS data or satellite observations, a registration of TLS to the  
832 UAV-LS point cloud is highly recommended. The integration of GNSS directly into TLS data collection now ensures that  
833 registered plot-level point clouds are aligned within a global coordinate system. This significantly facilitates the co-registration  
834 of TLS and UAV-LS point clouds, given that GNSS accuracy is typically within 1 metre. Historically, placing all LiDAR point  
835 clouds within accurate global coordinate systems necessitated dedicated survey measurements of plot corners or TLS locations  
836 via GNSS, a process often hindered by signal attenuation in dense forests. Consequently, GNSS surveying of plot corner  
837 locations is not a standard component of forest census protocols, although it should be considered essential for plots intended  
838 for EO calibration and validation purposes. The reduced cost of RTK GNSS equipment and its subsequent routine integration  
839 into TLS workflows have made this more feasible, despite the challenges in obtaining fixed positions, and maintaining radio  
840 link with a base positioned on a well-known point under deep forest canopy cover. While this may not benefit ALS directly,

841 UAV-LS is likely to serve as a valuable intermediary between TLS (and census data) and ALS. The requirement for global  
842 GNSS positioning also extends to other spatial datasets.

843 **3.3 Aligning TLS and UAV-LS to ALS data**

844 Aligning ALS data with TLS and UAV-LS datasets presents significant challenges. Despite the use of high-quality GNSS  
845 positioning, meter-scale geolocation discrepancies between sensors can occur. Co-locating LiDAR datasets acquired at  
846 different scales -TLS, UAV-LS, and ALS- remains complex, with no standard or “turn-key” solution currently available.  
847 Manual intervention is often required, and the approach varies by site and sensor combination. While plot-level AGB  
848 estimation is relatively tolerant to these discrepancies, finer-scale applications (e.g., matching to tree-level census data) demand  
849 more precise alignment. This can be partially addressed through manual co-registration using common tie points across  
850 datasets.

851 Achieving meaningful alignment also depends on the internal characteristics of ALS point clouds. Acquisition parameters such  
852 as point density, scan angle distribution, and footprint size influence comparability and should be controlled as far as possible.  
853 Post-processing can regularise point density and scan angles within or across campaigns, improving consistency.  
854 Homogeneous scanning geometry enables more stable structural metrics and enhances AGB prediction performance.  
855 Similarly, parameters such as transmitted pulse power (which co-varies with pulse repetition rate) and flight altitude (affecting  
856 footprint size and canopy penetration) should be standardised across acquisitions to minimise bias (Vincent et al., 2023). These  
857 steps are critical for reducing alignment errors and ensuring robust comparisons between TLS, UAV-LS, and ALS datasets.

859 **4. Recommendations for data collection in FBRMS**

860 Building on this first case study, we make the following general recommendations for data collection of tropical forest plot  
861 census, TLS, UAV-LS and ALS data for the specific application of estimating AGB and upscaling to EO estimates. These  
862 recommendations follow from the CEOS LPV AGB protocol and subsequent requirements identified for the GEO-TREES  
863 initiative.

864 • **Consistent data acquisition and processing:** in order to facilitate the comparison of AGB estimates between sites,  
865 dates, teams, etc. care should be taken to collect and process data as consistently as possible. This might seem obvious  
866 but is particularly important as the use of TLS and UAV-LS for AGB estimation (and even ALS in some cases) are  
867 currently primarily research-led (as opposed to fully operational). As new methods and tools are developed, including  
868 newer versions of existing software, care should be taken to ensure backwards compatibility of the resulting AGB  
869 estimates. This means either re-processing older data, or at the very least, some form of cross-comparison of original  
870 and new methods. In our experience, listed below are some of the areas where care is needed to ensure data  
871 consistency and reduce bias and uncertainty:

872     ● **TLS data acquisition** - comparison between sites and plots is made much easier by using the same census,  
 873     TLS, UAV-LS and ALS data acquisition and processing protocols. Even within the forest plot census  
 874     community there are slightly different protocols and processes between different plot networks. This is even  
 875     more variable for different sources of LiDAR data. We note that much of the TLS work in tropical forests  
 876     aimed at volume reconstruction and AGB estimation has been carried out with RIEGL VZ series TLS  
 877     instruments. We make no comment as to what is 'the best' instrument - there are various cost/benefit trade-  
 878     offs to be made. Equipment has to be robust to withstand tropical forest work (and humidity). LiDAR range  
 879     needs to be in the 100s of metres to ensure points are returned from tall canopies. Phase-shift TLS systems  
 880     can be light and have very rapid scan rates, but suffer from 'ghosting' of multiple returned hits along a beam  
 881     path. Mobile Laser Scanning (MLS) systems offer rapid coverage, and require minimal input for registration  
 882     by using simultaneous location and mapping (SLAM), but tend to have lower range and precision due to the  
 883     uncertainty in absolute location resulting from SLAM. It is likely that these systems will become more  
 884     powerful and precise, offering a possible alternative to static tripod-mounted TLS in the future for AGB  
 885     applications. Specific issues to consider are TLS power. For example, the RIEGL VZ-400 and newer VZ-  
 886     400i systems (both used here) have different recording sensitivities i.e. down to -30 dB for the newer VZ-  
 887     400i, whereas the VZ-400 only recorded to -20 dB. This can have a significant impact on the number of  
 888     returns, particularly from further away and higher in the canopy and should be taken into consideration when  
 889     comparing results between older and newer TLS instruments. Choices are also possible in terms of power  
 890     settings: lower power settings reduce scan times & extend battery time, but also significantly reduce the  
 891     quality of resulting point clouds, particularly higher in the canopy. TLS data were collected using a pulse  
 892     repetition rate (PRR) of 300 kHz on RIEGL VZ-400 and VZ-400i scanners, trading longer scan times for a  
 893     fixed angular resolution to maximise coverage at the tops of tall trees. In the RIEGL configuration, PRR and  
 894     emitted laser power are intrinsically linked: increasing the PRR reduces the available power, which in turn  
 895     decreases the maximum range of the scanner. At very high PRR settings, this reduction in range means that  
 896     the tops of tall trees may not be captured effectively. Therefore, selecting a lower PRR (300 kHz) ensures  
 897     sufficient power and range to cover the full canopy height of forests, while maintaining the desired angular  
 898     resolution.

899     However, recent work by Verheltz et al. (2024) suggests that using lower power, but with higher  
 900     angular resolution, can achieve better coverage in tall forests for the same scan duration (3 mins per scan).  
 901     More generally, comparing measurements made with scanners of varying power, sensitivity, resolution etc.  
 902     will compound uncertainties (particularly biases) in the resulting estimates of AGB and so should be avoided  
 903     or minimised as far as possible. This is particularly important for large-scale site-to-site comparison required  
 904     for EO biomass product cal/val (e.g. for global FBRMS comparisons).

905     ● **TLS processing** - broadly, TLS data acquisition and processing in tropical forests has gradually converged  
 towards something of a consensus, albeit this is still an active area of research and will vary depending on

**Deleted:**

**Deleted:** and vice versa

**Formatted:** Font: (Default) +Headings (Times New Roman)

**Deleted:** Consequently, the choice of PRR determines the power setting, and adjustments to one parameter necessarily influence the other.

911 the team, site and application. Specific issues to consider are the way in which trees are extracted from plot-  
912 scale point clouds. Currently, the most accurate method for doing this is by manual cleaning of each tree  
913 using a tool such as CloudCompare (CloudCompare Development Team, 2025). However, this is a time-  
914 consuming and somewhat subjective process that is not fully replicable - different people will produce  
915 slightly different results. Automated pipelines using machine learning/deep learning (ML/DL) offer a more  
916 rapid and repeatable approach (e.g. Krisanski et al., 2021; Wilkes et al., 2023), however, their resulting tree  
917 extraction accuracy is harder to assess given that the 'true' structure of trees is unknown. Manually-extracted  
918 trees can be used to assess automated tree extraction accuracy, as well as forming the training data to enable  
919 improvements in the underlying ML/DL approaches. Developing locally-trained / optimised ML/DL models  
920 is likely to improve this approach further. Moving from individual tree point clouds to volume estimates it  
921 is also important to use consistent QSM-fitting approaches. For example, there are systematic differences  
922 between older and newer versions of TreeQSM, currently the most widely-used QSM fitting software  
923 (Demol et al., 2024; Raumonen et al., 2013). Quantifying the uncertainty in tree-level estimates of volume  
924 will depend on this processing chain, which will then determine the plot-level uncertainty when upscaling.

- 925 • **UAV-LS acquisition and processing** - due to the wide range of platforms and LiDAR payloads being used  
926 (as well as local UAV and safety regulations), there is currently little consensus in terms of both acquisition  
927 and processing of UAV-LS data. There are a wide range of flight choices (particularly altitude), instrument  
928 settings (scan angle), and survey systems (overlap, duration, etc.) that are a function of platform  
929 performance, cost, etc. The impact of some of these choices is discussed in Brede et al. (2022b) where the  
930 benefits of higher power, multiple returns and overlapping flights in detecting canopy structure are  
931 highlighted. UAV-LS is not a like-for-like replacement for TLS, thus, the ability to compare these two  
932 different sources of LiDAR data will be facilitated by accurate geo-location (see above). This can be  
933 achieved by using ground targets with surveyed locations that can be identified in the UAV-LS data (e.g.  
934 reflective sheets/tarps, umbrellas, commercial UAV targets etc). This presupposes that there are sufficient  
935 gaps in the canopy for targets to be seen, which is not always true. During data collection attention should  
936 be paid to also either have access to GNSS observables from permanent base stations (e.g. CORS network)  
937 or collect observables with a temporary base station (e.g. Emlid Reach RS+ or RS2). A base station should  
938 be positioned less than 15 km away from the survey area. An important consideration for UAV-LS data  
939 collection is whether visual line of sight VLOS needs to be maintained, i.e. visibility of the platform by the  
940 pilot during the whole mission. If so, this can impact the choice of take-off, flight plan, etc. which in turn  
941 may influence the choice of platform. Fixed-wing platforms have a much greater area coverage and flight  
942 duration than VTOL platforms, but by necessity, must operate beyond VLOS (BVLOS). They also require  
943 far more space to take off and land than VTOL platforms.

944     ● **ALS acquisition and processing** - while ALS has been used operationally for forest applications for several  
945       decades, its application for AGB estimates specifically is still less well-defined. In particular, this is true  
946       when considering tree-scale rather than plot-level estimates. Practically, ALS surveys are almost always  
947       outsourced (from the plot PIs, census and TLS, UAV teams) to commercial or agency (e.g. NASA, ESA,  
948       NERC) providers. In the former case, there may be limited input from the end user over the platform,  
949       instrument and acquisition parameters, or the way in which the data are processed to the resulting final  
950       delivery. In ESA, NERC, NASA acquisitions, there tends to be more input from the users, but there may be  
951       other restrictions in terms of when and where flights can be made. We recommend a pulse density of  $10 \text{ m}^{-2}$   
952       or higher and a swath angle of +/-15 degrees or smaller. Most importantly, consistency over time of the  
953       other acquisition parameters should be sought to enable meaningful temporal analysis of ALS point cloud.  
954       In most cases, the 3D point cloud will be processed to generate a 2D canopy height model for further analysis.  
955       This post-processing can have important effects on the results, we therefore, recommend users follow a  
956       standardized procedure such as Fischer et al. (2024).

957     ● **Accurate (cm-scale) GNSS locations for 1ha FBRMS plot corners (or at the least the nominal origin 0, 0  
958       coordinate for each plot):** this makes comparison and merging of any subsequent measurements much easier. It is  
959       important to note that this is not a standard requirement of forest census measurements and requires specialist  
960       surveying equipment e.g. GNSS RTK base station + rover configuration. It is also challenging under heavy forest  
961       cover. Given that such setups are required (ideally) for TLS and UAV-LS, plot corner surveying is potentially best  
962       carried out by these teams.

963     ● **Linking TLS trees to their census counterparts:** ideally, a permanent  $10 \times 10\text{m}$  subplot grid would be established  
964       within each 1 ha forest plot. Census teams can then follow the same chain sampling pattern used in TLS data collection  
965       (see Figure 2.1.4b & c) and identify the tree IDs found within each  $10 \times 10\text{m}$  quadrants as they move through the  
966       plot. However, placing a  $10 \times 10\text{m}$  sub-grid is not always straightforward (or even desirable) as it may require rebar  
967       posts, which can be expensive and are likely to be removed or damaged by e.g. elephants in West African plots  
968       particularly. An alternative approach is to label some trees with temporary numbered QR-type markers that can be  
969       read automatically from the lidar point cloud data. The markers can be printed on A4 waterproof paper, attached to  
970       trees with known census ID, and then identified in the TLS data using a tool such as qrDAR (Wilkes et al., 2017). If  
971       the 20 or so largest trees are labelled in this way, distributed across a 1 ha plot, this makes subsequent tree matching  
972       between census and TLS data much easier as there are known ‘anchor trees’ for the survey team to work from.

973     **5. Data Access**

974     This paper presents 30 datasets, comprising LiDAR and tree census data for all three ForestScan FBRMS. All datasets are  
975       archived and publicly accessible through established data repositories. LiDAR datasets, including TLS, UAV-LS and ALS are

976 freely available from the CEDA Archive (<https://archive.ceda.ac.uk>) under the ForestScan data collection  
977 (<https://dx.doi.org/10.5285/88a8620229014e0ebacf0606b302112d>; Chavana-Bryant et al., 2025b). This collection serves as  
978 an umbrella repository linking all individual LiDAR datasets by site and acquisition type. All tree census datasets are provided  
979 as curated data packages made available by the ForestPlots consortium and the French Agricultural Research Centre for  
980 International Development (CIRAD) open-access portal.

981  
982 Tree census data packages for all three FBRMS are made available via two archival platforms: the CIRAD DataVerse portal  
983 for French Guiana (<https://dataVERSE.cirad.fr/dataset.xhtml?persistentId=doi:10.18167/DVN1/94XHID>; Derroire et al., 2025),  
984 while Gabon and Malaysian Borneo data are available through ForestPlots.net ([https://doi.org/10.5521/forestplots.net/2025\\_2](https://doi.org/10.5521/forestplots.net/2025_2);  
985 Chavana-Bryant et al., 2025a). An additional census dataset for a non-ForestScan plot at FBRMS-01 is included in Table 10  
986 and made available via the CEDA archive.

987  
988 Both tree census archival platforms operate under a fair use policy, governed by the Creative Commons Attribution-  
989 NonCommercial-ShareAlike 4.0 International Licence (CC BY-NC-SA 4.0) (see <https://forestplots.net/en/join-forestplots/working-with-data> and <https://dataVERSE.org/best-practices/dataVERSE-community-norms>). These policies reflect a  
990 strong commitment to equitable and inclusive data collection, funding, and sharing practices, as outlined in the ForestPlots  
991 code of conduct (<https://forestplots.net/en/join-forestplots/code-of-conduct>). Tropical forest plot census data provide unique  
992 insights into forest structure and dynamics but are challenging and often hazardous to collect, requiring sustained investment  
993 and logistical support in remote regions with limited infrastructure. A persistent challenge to equitable research is that those  
994 who collect these data are often least able to exploit the resulting large-scale datasets. This issue is particularly acute in the  
995 context of commercial data exploitation, including by artificial intelligence and large-scale data mining enterprises. To address  
996 this, the ForestPlots community has developed data-sharing agreements that promote fairness and inclusivity, as detailed in de  
997 Lima et al. (2022).

998  
1000 Access and citation details for all ForestScan datasets are organised by site in Tables 10, 11, and 12 for FBRMS-01: Paracou,  
1001 French Guiana, FBRMS-02: Lopé National Park, Gabon, and FBRMS-03: Sepilok-Kabili, Malaysian Borneo, respectively.  
1002 Each table provides the specific data type, acquisition date, license type and citation format including DOI and URL for each  
1003 individual ForestScan dataset.

1004  
1005 **Table 10:** Dataset type, acquisition date, license type, and citation format including DOI and URL details for LiDAR (TLS,  
1006 UAV-LS and ALS) and tree census datasets available for FBRMS-01: Paracou, French Guiana. When using any of the  
1007 ForestScan datasets, this paper must also be cited.

ForestScan French Guiana Datasets / Acquisition date / Data license type	Data type	Citable as (DOI and URL included)
---	-----------	-----------------------------------

→ Formatted Table

ForestScan Collection	Collection (multi-type composite of all ForestScan CEDA datasets)	Chavana-Bryant, C.; Wilkes, P.; Yang, W.; Burt, A.; Vines, P.; Bennett, A.C.; Pickavance, G.C.; Cooper, D.L.M.; Lewis, S.L.; Phillips, O.L.; Brede, B.; Lau, A.; Herold, M.; McNicol, I.M.; Mitchard, E.T.A.; Coombes, D.; Jackson, T.D.; Makaga, L.; Milamizokou Napo, H.O.; Ngomanda, A.; Ntie, S.; Medjibe, V.; Dimbonda, P.; Soenens, L.; Daelemans, V.; Proux, L.; Nilus, R.; Labrière, N.; Jeffery, K.; Burslem, D.F.R.P.; Clewley, D.; Moffat, D.; Qie, L.; Bartholomeus, H.; Vincent, G.; Barbier, N.; Derroire, G.; Abernethy, K.; Scipal, K.; Disney, M. (2025): ForestScan Collection. NERC EDS Centre for Environmental Data Analysis, 20 January 2025. DOI:10.5285/88a8620229014e0ebacf0606b302112d. <a href="https://catalogue.ceda.ac.uk/uuid/88a8620229014e0ebacf0606b302112d">https://catalogue.ceda.ac.uk/uuid/88a8620229014e0ebacf0606b302112d</a>
ForestScan Project: Terrestrial Laser Scanning (TLS) of FBRMS-01: Paracou, French Guiana 1ha plot FG5c1  Acquisition date: Sep - Oct 2022  License type: CC BY 4.0 <a href="http://creativecommons.org/licenses/by/4.0/">http://creativecommons.org/licenses/by/4.0/</a>	TLS	Chavana-Bryant, C.; Wilkes, P.; Yang, W.; Burt, A.; Vines, P.; Bennett, A.C.; Pickavance, G.C.; Cooper, D.L.M.; Lewis, S.L.; Phillips, O.L.; Brede, B.; Lau, A.; Herold, M.; McNicol, I.M.; Mitchard, E.T.A.; Coombes, D.; Jackson, T.D.; Makaga, L.; Milamizokou Napo, H.O.; Ngomanda, A.; Ntie, S.; Medjibe, V.; Dimbonda, P.; Soenens, L.; Daelemans, V.; Proux, L.; Nilus, R.; Labrière, N.; Jeffery, K.; Burslem, D.F.R.P.; Clewley, D.; Moffat, D.; Qie, L.; Bartholomeus, H.; Vincent, G.; Barbier, N.; Derroire, G.; Abernethy, K.; Scipal, K.; Disney, M. (2025): ForestScan Project : Terrestrial Laser Scanning (TLS) of FBRMS-01: Paracou, French Guiana 1ha plot FG5c1, September to October 2022. NERC EDS Centre for Environmental Data Analysis, 28 March 2025. DOI:10.5285/656ac8ee1d42443f9addcbce28c1b137. <a href="https://dx.doi.org/10.5285/656ac8ee1d42443f9addcbce28c1b137">https://dx.doi.org/10.5285/656ac8ee1d42443f9addcbce28c1b137</a>
ForestScan Project: Terrestrial Laser Scanning (TLS) of FBRMS-01: Paracou, French Guiana 1ha plot FG6c2  Acquisition date: Sep - Oct 2022  License type: CC BY 4.0 <a href="http://creativecommons.org/licenses/by/4.0/">http://creativecommons.org/licenses/by/4.0/</a>	TLS	Chavana-Bryant, C.; Wilkes, P.; Yang, W.; Burt, A.; Vines, P.; Bennett, A.C.; Pickavance, G.C.; Cooper, D.L.M.; Lewis, S.L.; Phillips, O.L.; Brede, B.; Lau, A.; Herold, M.; McNicol, I.M.; Mitchard, E.T.A.; Coombes, D.; Jackson, T.D.; Makaga, L.; Milamizokou Napo, H.O.; Ngomanda, A.; Ntie, S.; Medjibe, V.; Dimbonda, P.; Soenens, L.; Daelemans, V.; Proux, L.; Nilus, R.; Labrière, N.; Jeffery, K.; Burslem, D.F.R.P.; Clewley, D.; Moffat, D.; Qie, L.; Bartholomeus, H.; Vincent, G.; Barbier, N.; Derroire, G.; Abernethy, K.; Scipal, K.; Disney, M. (2025): ForestScan Project : Terrestrial Laser Scanning (TLS) of FBRMS-01: Paracou, French Guiana 1ha

		plot FG6c2, September to October 2022. NERC EDS Centre for Environmental Data Analysis, 28 March 2025. DOI:10.5285/931973db09af41568853702efe135f29. <a href="https://dx.doi.org/10.5285/931973db09af41568853702efe135f29">https://dx.doi.org/10.5285/931973db09af41568853702efe135f29</a>
ForestScan Project: Terrestrial Laser Scanning (TLS) of FBRMS-01: Paracou, French Guiana 1ha plot FG8c4  Acquisition date: Sep - Oct 2022  License type: CC BY 4.0 <a href="http://creativecommons.org/licenses/by/4.0/">http://creativecommons.org/licenses/by/4.0/</a>	TLS	Chavana-Bryant, C.; Wilkes, P.; Yang, W.; Burt, A.; Vines, P.; Bennett, A.C.; Pickavance, G.C.; Cooper, D.I.M.; Lewis, S.L.; Phillips, O.L.; Brede, B.; Lau, A.; Herold, M.; McNicol, I.M.; Mitchard, E.T.A.; Coombes, D.; Jackson, T.D.; Makaga, L.; Milamizokou Napo, H.O.; Ngomanda, A.; Ntie, S.; Medjibe, V.; Dimbonda, P.; Soenens, L.; Daelemans, V.; Proux, L.; Nilus, R.; Labrière, N.; Jeffery, K.; Burslem, D.F.R.P.; Clewley, D.; Moffat, D.; Qie, L.; Bartholomeus, H.; Vincent, G.; Barbier, N.; Derroire, G.; Abernethy, K.; Scipal, K.; Disney, M. (2025): ForestScan Project : Terrestrial Laser Scanning (TLS) of FBRMS-01: Paracou, French Guiana 1ha plot FG8c4, September to October 2022. NERC EDS Centre for Environmental Data Analysis, 28 March 2025. DOI:10.5285/40f0f38023ac40f6b40bbf96e4dc5258. <a href="https://dx.doi.org/10.5285/40f0f38023ac40f6b40bbf96e4dc5258">https://dx.doi.org/10.5285/40f0f38023ac40f6b40bbf96e4dc5258</a>
ForestScan: Terrestrial Laser Scanning (TLS) of FBRMS-01: Paracou, French Guiana 1ha plot IRD-CNES (Tropiscat)  Acquisition date: Oct 2021  License type: CC BY 4.0 <a href="http://creativecommons.org/licenses/by/4.0/">http://creativecommons.org/licenses/by/4.0/</a>	TLS	Vincent, G.; Villard, L. (2025): ForestScan: Terrestrial Laser Scanning (TLS) of FBRMS-01: Paracou, French Guiana 1ha plot IRD-CNES, October 2021. NERC EDS Centre for Environmental Data Analysis, 28 March 2025. DOI:10.5285/b1cd34f6af7941a3b1429ac52a3f6b28. <a href="https://dx.doi.org/10.5285/b1cd34f6af7941a3b1429ac52a3f6b28">https://dx.doi.org/10.5285/b1cd34f6af7941a3b1429ac52a3f6b28</a>
ForestScan Project: Unpiloted Aerial Vehicle LiDAR Scanning (UAV-LS) and Terrestrial Laser Scanning (TLS) data of FBRMS-01: Paracou, French Guiana plot 6  Acquisition date: Oct – Nov 2019  License type: CC BY 4.0 <a href="http://creativecommons.org/licenses/by/4.0/">http://creativecommons.org/licenses/by/4.0/</a>	UAV-LS + TLS	Brede, B.; Barbier, N.; Bartholomeus, H.; Derroire, G.; Lau, A.; Lusk, D.; Herold, M. (2025): ForestScan Project: Unpiloted Aerial Vehicle LiDAR Scanning (UAV-LS) and Terrestrial Laser Scanning (TLS) data of FBRMS-01: Paracou, French Guiana plot 6, 10th October to 15th November 2019. NERC EDS Centre for Environmental Data Analysis, 28 March 2025. DOI:10.5285/325a4dde60d142049339e0c84816aac1. <a href="https://dx.doi.org/10.5285/325a4dde60d142049339e0c84816aac1">https://dx.doi.org/10.5285/325a4dde60d142049339e0c84816aac1</a>
ForestScan Project: Multiple Unpiloted Aerial Vehicle LiDAR Scanning (UAV-LS) data acquisitions of FBRMS-	UAV-LS	Barbier, N.; Vincent, G. (2025): ForestScan Project: Multiple Unpiloted Aerial Vehicle LiDAR Scanning (UAV-LS) data acquisitions of FBRMS-01: Paracou,

01: Paracou, French Guiana, plots 4, 5, 6, 8, IRD-CNES (Tropiscat) and Flux-Tower area  Acquisition date: Oct 2019  License type: CC BY 4.0 <a href="http://creativecommons.org/licenses/by/4.0/">http://creativecommons.org/licenses/by/4.0/</a>		French Guiana, plots 4, 5, 6, 8, IRD-CNES and Flux-Tower area, October 2019. NERC EDS Centre for Environmental Data Analysis, 28 March 2025. DOI:10.5285/005f2e0aebc24ed98a9772a0ba3798e2. <a href="https://dx.doi.org/10.5285/005f2e0aebc24ed98a9772a0ba3798e2">https://dx.doi.org/10.5285/005f2e0aebc24ed98a9772a0ba3798e2</a>
ForestScan: Aerial Laser Scanning (ALS) of FBRMS-01: Paracou, French Guiana  Acquisition date: Nov 2022  License type: CC BY 4.0 <a href="http://creativecommons.org/licenses/by/4.0/">http://creativecommons.org/licenses/by/4.0/</a>	ALS	Vincent, G. (2025): ForestScan: Aerial Laser Scanning (ALS) of FBRMS-01: Paracou, French Guiana, November 2022. NERC EDS Centre for Environmental Data Analysis, 28 March 2025. DOI:10.5285/7bef89a9dc404683a46642625a024a4b. <a href="https://dx.doi.org/10.5285/7bef89a9dc404683a46642625a024a4b">https://dx.doi.org/10.5285/7bef89a9dc404683a46642625a024a4b</a>
Aerial LiDAR (ALS) French Guiana Paracou  Acquisition date: Nov 2019  License type: CC BY 4.0 <a href="http://creativecommons.org/licenses/by/4.0/">http://creativecommons.org/licenses/by/4.0/</a>	ALS	Jackson, T.D.; Vincent, G.; Coomes, D.A. (2023): Aerial LiDAR data from French Guiana, Paracou, November 2019. NERC EDS Centre for Environmental Data Analysis, 20 December 2023. DOI:10.5285/1d554ff41c104491ac3661c6ff52aab. <a href="https://dx.doi.org/10.5285/1d554ff41c104491ac3661c6ff52aab">https://dx.doi.org/10.5285/1d554ff41c104491ac3661c6ff52aab</a>
Aerial LiDAR (ALS) French Guiana Nouragues  Acquisition date: Nov 2019  License type: CC BY 4.0 <a href="http://creativecommons.org/licenses/by/4.0/">http://creativecommons.org/licenses/by/4.0/</a>	ALS (additional non- ForestScan plot)	Jackson, T.D.; Vincent, G.; Coomes, D.A. (2023): Aerial LiDAR data from French Guiana, Nouragues, November 2019. NERC EDS Centre for Environmental Data Analysis, 20 December 2023. DOI:10.5285/7bdc5fc06264802be34f918597150e8. <a href="https://dx.doi.org/10.5285/7bdc5fc06264802be34f918597150e8">https://dx.doi.org/10.5285/7bdc5fc06264802be34f918597150e8</a>
ForestScan: Plot descriptions for FBRMS-01: Paracou, French Guiana, 1ha plots FG5c1, FG6c2 and FG8c4  License: CC BY-NC-SA 4.0 <a href="http://creativecommons.org/licenses/by-nc-sa/4.0/">http://creativecommons.org/licenses/by-nc-sa/4.0/</a>	Tree census plot descriptions	Derroire, G., Héault, B., Rossi, V., Blanc, L., Gourlet-Fleury, S., Schmitt, L., 2025, "ForestScan", 10.18167/DVN1/94XHID, CIRAD Dataverse, V1 <a href="https://dataverse.cirad.fr/dataset.xhtml?persistentId=doi:10.18167/DVN1/94XHID">https://dataverse.cirad.fr/dataset.xhtml?persistentId=doi:10.18167/DVN1/94XHID</a>
ForestScan: Tree census data for FBRMS-01: Paracou, French Guiana, 1ha plots FG5c1, FG6c2 and FG8c4  Acquisition date: FG5c1: Aug 2023 FG6c2: May - Jun 2023 FG8c4: Sep 2023	Tree census	Derroire, G., Héault, B., Rossi, V., Blanc, L., Gourlet-Fleury, S., Schmitt, L., 2025, "ForestScan", 10.18167/DVN1/94XHID, CIRAD Dataverse, V1 <a href="https://dataverse.cirad.fr/dataset.xhtml?persistentId=doi:10.18167/DVN1/94XHID">https://dataverse.cirad.fr/dataset.xhtml?persistentId=doi:10.18167/DVN1/94XHID</a>

License: CC BY-NC-SA 4.0 <a href="http://creativecommons.org/licenses/by-nc-sa/4.0/">http://creativecommons.org/licenses/by-nc-sa/4.0/</a>		
ForestScan: Tree census data (diameter and species name) of FBRMS-01: Paracou, French Guiana 1ha plot IRD-CNES (Tropiscat)  Acquisition date: Oct 2021  License type: CC BY 4.0 <a href="http://creativecommons.org/licenses/by/4.0/">http://creativecommons.org/licenses/by/4.0/</a>	Tree census (additional non-ForestScan plot)	Vincent, G.; Martin, O.; Engel, F. (2025): ForestScan: Tree census data (diameter and species name) of FBRMS-01: Paracou, French Guiana 1ha plot IRD-CNES, October 2021. NERC EDS Centre for Environmental Data Analysis. <i>28 March 2025</i> . DOI:10.5285/5e78ff91e9cd4143bfa3b7358efd2607. <a href="https://dx.doi.org/10.5285/5e78ff91e9cd4143bfa3b7358efd2607">https://dx.doi.org/10.5285/5e78ff91e9cd4143bfa3b7358efd2607</a>

1008

1009

1010

1011

**Table 10:** Dataset type, acquisition date, license type, and citation format including DOI and URL details for LiDAR (TLS, UAV-LS and ALS) and tree census datasets available for FBRMS-02: Lopé, Gabon. When using any of the ForestScan datasets, this paper must also be cited.

ForestScan Gabon Datasets / Acquisition date / Data license type	Data type	Citable as (DOI and URL included)
ForestScan Project : Terrestrial Laser Scanning (TLS) of FBRMS-02: Station d'Etudes des Gorilles et Chimpanzés, Lopé National Park, Gabon 1ha plot LPG-01  Acquisition date: Jun - Jul 2022  License type: CC BY 4.0 <a href="http://creativecommons.org/licenses/by/4.0/">http://creativecommons.org/licenses/by/4.0/</a>	TLS	Chavana-Bryant, C.; Wilkes, P.; Yang, W.; Burt, A.; Vines, P.; Bennett, A.C.; Pickavance, G.C.; Cooper, D.L.M.; Lewis, S.L.; Phillips, O.L.; Brede, B.; Lau, A.; Herold, M.; McNicol, I.M.; Mitchard, E.T.A.; Coombes, D.; Jackson, T.D.; Makaga, L.; Milamizokou Napo, H.O.; Ngomanda, A.; Ntie, S.; Medjibe, V.; Dimbonda, P.; Soenens, L.; Daelemans, V.; Proux, L.; Nilus, R.; Labrière, N.; Jeffery, K.; Burslem, D.F.R.P.; Clewley, D.; Moffat, D.; Qie, L.; Bartholomeus, H.; Vincent, G.; Barbier, N.; Derroire, G.; Abernethy, K.; Scipal, K.; Disney, M. (2025): ForestScan Project : Terrestrial Laser Scanning (TLS) of FBRMS-02: Station d'Etudes des Gorilles et Chimpanzés, Lopé National Park, Gabon 1ha plot LPG-01, June to July 2022. NERC EDS Centre for Environmental Data Analysis. <i>28 March 2025</i> . DOI:10.5285/8ea2c697ee53430a84825384bfdcf06a. <a href="https://dx.doi.org/10.5285/8ea2c697ee53430a84825384bfdcf06a">https://dx.doi.org/10.5285/8ea2c697ee53430a84825384bfdcf06a</a>
ForestScan Project : Terrestrial Laser Scanning (TLS) of FBRMS-02: Station d'Etudes des Gorilles et Chimpanzés, Lopé National Park, Gabon 1ha plot OKO-01  Acquisition date: Jun - Jul 2022	TLS	Chavana-Bryant, C.; Wilkes, P.; Yang, W.; Burt, A.; Vines, P.; Bennett, A.C.; Pickavance, G.C.; Cooper, D.L.M.; Lewis, S.L.; Phillips, O.L.; Brede, B.; Lau, A.; Herold, M.; McNicol, I.M.; Mitchard, E.T.A.; Coombes, D.; Jackson, T.D.; Makaga, L.; Milamizokou Napo, H.O.; Ngomanda, A.; Ntie, S.;

Formatted Table

<p>License type: CC BY 4.0  <a href="http://creativecommons.org/licenses/by/4.0/">http://creativecommons.org/licenses/by/4.0/</a></p>		<p>Medjibe, V.; Dimbonda, P.; Soenens, L.; Daelemans, V.; Proux, L.; Nilus, R.; Labrière, N.; Jeffery, K.; Burslem, D.F.R.P.; Clewley, D.; Moffat, D.; Qie, L.; Bartholomeus, H.; Vincent, G.; Barbier, N.; Derroire, G.; Abernethy, K.; Scipal, K.; Disney, M. (2025): ForestScan Project : Terrestrial Laser Scanning (TLS) of FBRMS-02: Station d'Etudes des Gorilles et Chimpanzés, Lopé National Park, Gabon 1ha plot OKO-01, June to July 2022. NERC EDS Centre for Environmental Data Analysis, 28 March 2025. DOI:10.5285/45ae3437f82f4e4fb759a5c26a194ba. <a href="https://dx.doi.org/10.5285/45ae3437f82f4e4fb759a5c26a194ba">https://dx.doi.org/10.5285/45ae3437f82f4e4fb759a5c26a194ba</a></p>
<p>ForestScan Project : Terrestrial Laser Scanning (TLS) of FBRMS-02: Station d'Etudes des Gorilles et Chimpanzés, Lopé National Park, Gabon 1ha plot OKO-02</p> <p>Acquisition date: Jun - Jul 2022</p> <p>License type: CC BY 4.0  <a href="http://creativecommons.org/licenses/by/4.0/">http://creativecommons.org/licenses/by/4.0/</a></p>	<p><a href="#">TLS</a></p>	<p>Chavana-Bryant, C.; Wilkes, P.; Yang, W.; Burt, A.; Vines, P.; Bennett, A.C.; Pickavance, G.C.; Cooper, D.L.M.; Lewis, S.L.; Phillips, O.L.; Brede, B.; Lau, A.; Herold, M.; McNicol, I.M.; Mitchard, E.T.A.; Coombes, D.; Jackson, T.D.; Makaga, L.; Milamizokou Napo, H.O.; Ngomanda, A.; Ntie, S.; Medjibe, V.; Dimbonda, P.; Soenens, L.; Daelemans, V.; Proux, L.; Nilus, R.; Labrière, N.; Jeffery, K.; Burslem, D.F.R.P.; Clewley, D.; Moffat, D.; Qie, L.; Bartholomeus, H.; Vincent, G.; Barbier, N.; Derroire, G.; Abernethy, K.; Scipal, K.; Disney, M. (2025): ForestScan Project : Terrestrial Laser Scanning (TLS) of FBRMS-02: Station d'Etudes des Gorilles et Chimpanzés, Lopé National Park, Gabon 1ha plot OKO-02, June to July 2022. NERC EDS Centre for Environmental Data Analysis, 28 March 2025. DOI:10.5285/f4b43475c9641cca1dad2c8be8dadaf. <a href="https://dx.doi.org/10.5285/f4b43475c9641cca1dad2c8be8dadaf">https://dx.doi.org/10.5285/f4b43475c9641cca1dad2c8be8dadaf</a></p>
<p>ForestScan Project : Terrestrial Laser Scanning (TLS) of FBRMS-02: Station d'Etudes des Gorilles et Chimpanzés, Lopé National Park, Gabon 1ha plot OKO-03</p> <p>Acquisition date: Jun - Jul 2022</p> <p>License type: CC BY 4.0  <a href="http://creativecommons.org/licenses/by/4.0/">http://creativecommons.org/licenses/by/4.0/</a></p>	<p><a href="#">TLS</a></p>	<p>Chavana-Bryant, C.; Wilkes, P.; Yang, W.; Burt, A.; Vines, P.; Bennett, A.C.; Pickavance, G.C.; Cooper, D.L.M.; Lewis, S.L.; Phillips, O.L.; Brede, B.; Lau, A.; Herold, M.; McNicol, I.M.; Mitchard, E.T.A.; Coombes, D.; Jackson, T.D.; Makaga, L.; Milamizokou Napo, H.O.; Ngomanda, A.; Ntie, S.; Medjibe, V.; Dimbonda, P.; Soenens, L.; Daelemans, V.; Proux, L.; Nilus, R.; Labrière, N.; Jeffery, K.; Burslem, D.F.R.P.; Clewley, D.; Moffat, D.; Qie, L.; Bartholomeus, H.; Vincent, G.; Barbier, N.; Derroire, G.; Abernethy, K.; Scipal, K.; Disney, M. (2025): ForestScan Project : Terrestrial Laser Scanning (TLS) of FBRMS-02: Station d'Etudes des Gorilles et Chimpanzés, Lopé National Park, Gabon 1ha plot OKO-03, June to July 2022. NERC EDS Centre for Environmental Data Analysis, 28 March 2025.</p>

		DOI:10.5285/8ed3ddec76b8470285bdb2ea643f54bc. <a href="https://dx.doi.org/10.5285/8ed3ddec76b8470285bdb2ea643f54bc">https://dx.doi.org/10.5285/8ed3ddec76b8470285bdb2ea643f54bc</a>
ForestScan project: Unpiloted Aerial Vehicle LiDAR Scanning (UAV-LS) data of FBRMS-02: Station d'Etudes des Gorilles et Chimpanzés, Lopé National Park, Gabon	<a href="#">UAV-LS</a>	McNicol, I.M.; Mitchard, E.T.A. (2025): ForestScan project: Unpiloted Aerial Vehicle LiDAR Scanning (UAV-LS) data of FBRMS-02: Station d'Etudes des Gorilles et Chimpanzés, Lopé National Park, Gabon, June 2022. NERC EDS Centre for Environmental Data Analysis, 28 March 2025. DOI: 10.5285/a79fc9ab0c443fc86d453cc064759b1. <a href="https://dx.doi.org/10.5285/a79fc9ab0c443fc86d453cc064759b1">https://dx.doi.org/10.5285/a79fc9ab0c443fc86d453cc064759b1</a>
Acquisition date: Jun 2022  License type: CC BY 4.0 <a href="http://creativecommons.org/licenses/by/4.0/">http://creativecommons.org/licenses/by/4.0/</a>		

ForestScan: Tree census data for FBRMS-02: Lope, Gabon, 1ha plots LPG-01, OKO-01, OKO-02 and OKO-03	Tree census	Chavana-Bryant, C., Wilkes, P., Yang, W., Burt, A., Vines, P., Bennett, A.C., Pickavance, G., Cooper, D.L.M., Lewis, S.L., Phillips, O.L., Brede, B., Lau, A., Herold, M., McNicol, I.M., Mitchard, E.T.A., Barbier, N., Vincent, G., Coomes, D.A., Jackson, T., Makaga, L., Milamizokou Napo, H.O., Ngomanda, A., Ntie, S., Medjibe, V., Dimbonda, P., Soenens, L., Daelemans, V., Bartholomeus, H., Majalap, N., Nilus, R., Labrière, N., Burslem, D.F.R.P., Qie, L., Derroire, G., Proux, L., Abernethy, K., Jeffery, K., Clewley, D., Moffat, D., Scipal, K. and Disney, M. ForestScan: a unique multiscale dataset of tropical forest structure across 3 continents including terrestrial, UAV and airborne LiDAR and in-situ forest census data. ESSD. 2025 DOI: <a href="https://doi.org/10.5521/forestplots.net/2025_2">10.5521/forestplots.net/2025_2</a> <a href="https://doi.org/10.5521/forestplots.net/2025_2">https://doi.org/10.5521/forestplots.net/2025_2</a>
Acquisition date: LPG-01: Feb 2022 OKO-01: Mar 2022 OKO-02: Feb 2022 OKO-03: Feb 2022  License: CC BY-NC-SA 4.0 <a href="http://creativecommons.org/licenses/by-nc-sa/4.0/">http://creativecommons.org/licenses/by-nc-sa/4.0/</a>		

1012

1013 **Table 11:** Dataset type, acquisition date, license type, and citation format including DOI and URL details for LiDAR (TLS,  
 1014 UAV-LS and ALS) and tree census datasets available for FBRMS-03: Kabili-Sepilok, Malaysian Borneo. When using any of  
 1015 the ForestScan datasets, this paper must also be cited.

ForestScan Malaysian Borneo Datasets / Acquisition date / Data license type	Data type	Citable as (DOI and URL included)
ForestScan Project : Terrestrial Laser Scanning (TLS) of FBRMS-03: Kabili-Sepilok, Malaysian Borneo 1ha plot SEP-11  Acquisition date: Mar 2017  License type: CC BY 4.0	<a href="#">TLS</a>	Chavana-Bryant, C.; Wilkes, P.; Yang, W.; Burt, A.; Vines, P.; Bennett, A.C.; Pickavance, G.C.; Cooper, D.L.M.; Lewis, S.L.; Phillips, O.L.; Brede, B.; Lau, A.; Herold, M.; McNicol, I.M.; Mitchard, E.T.A.; Coombes, D.; Jackson, T.D.; Makaga, L.; Milamizokou Napo, H.O.; Ngomanda, A.; Ntie, S.; Medjibe, V.; Dimbonda, P.; Soenens, L.; Daelemans, V.; Proux, L.; Nilus, R.; Labrière, N.; Jeffery, K.;

1016 Formatted Table

<p><a href="http://creativecommons.org/licenses/by/4.0/">http://creativecommons.org/licenses/by/4.0/</a></p>		<p>Burslem, D.F.R.P.; Clewley, D.; Moffat, D.; Qie, L.; Bartholomeus, H.; Vincent, G.; Barbier, N.; Derroire, G.; Abernethy, K.; Scipal, K.; Disney, M. (2025): ForestScan Project : Terrestrial Laser Scanning (TLS) of FBRMS-03: Kabili-Sepilok, Malaysian Borneo 1ha plot SEP-11, March 2017. NERC EDS Centre for Environmental Data Analysis, <i>28 March 2025</i>. DOI:10.5285/37b039605e9b4bb5a89371fd7f5b7ba1. <a href="https://dx.doi.org/10.5285/37b039605e9b4bb5a89371fd7f5b7ba1">https://dx.doi.org/10.5285/37b039605e9b4bb5a89371fd7f5b7ba1</a></p>
<p>ForestScan Project : Terrestrial Laser Scanning (TLS) of FBRMS-03: Kabili-Sepilok, Malaysian Borneo 1ha plot SEP-12</p> <p>Acquisition date: Mar 2017</p> <p>License type: CC BY 4.0 <a href="http://creativecommons.org/licenses/by/4.0/">http://creativecommons.org/licenses/by/4.0/</a></p>	<p><a href="#">TLS</a></p>	<p>Chavana-Bryant, C.; Wilkes, P.; Yang, W.; Burt, A.; Vines, P.; Bennett, A.C.; Pickavance, G.C.; Cooper, D.I.M.; Lewis, S.L.; Phillips, O.L.; Brede, B.; Lau, A.; Herold, M.; McNicol, I.M.; Mitchard, E.T.A.; Coombes, D.; Jackson, T.D.; Makaga, L.; Milamizokou Napo, H.O.; Ngomanda, A.; Ntie, S.; Medjibe, V.; Dimbonda, P.; Soenens, L.; Daelemans, V.; Proux, L.; Nilus, R.; Labrière, N.; Jeffery, K.; Burslem, D.F.R.P.; Clewley, D.; Moffat, D.; Qie, L.; Bartholomeus, H.; Vincent, G.; Barbier, N.; Derroire, G.; Abernethy, K.; Scipal, K.; Disney, M. (2025): ForestScan Project : Terrestrial Laser Scanning (TLS) of FBRMS-03: Kabili-Sepilok, Malaysian Borneo 1ha plot SEP-12, March 2017. NERC EDS Centre for Environmental Data Analysis, <i>28 March 2025</i>. DOI:10.5285/bb81c82352524df99ddd411f6ca2ec81. <a href="https://dx.doi.org/10.5285/bb81c82352524df99ddd411f6ca2ec81">https://dx.doi.org/10.5285/bb81c82352524df99ddd411f6ca2ec81</a></p>
<p>ForestScan Project: Terrestrial Laser Scanning (TLS) of FBRMS-03: Kabili-Sepilok, Malaysian Borneo 1ha plot SEP-30</p> <p>Acquisition date: Mar 2017</p> <p>License type: CC BY 4.0 <a href="http://creativecommons.org/licenses/by/4.0/">http://creativecommons.org/licenses/by/4.0/</a></p>	<p><a href="#">TLS</a></p>	<p>Chavana-Bryant, C.; Wilkes, P.; Yang, W.; Burt, A.; Vines, P.; Bennett, A.C.; Pickavance, G.C.; Cooper, D.I.M.; Lewis, S.L.; Phillips, O.L.; Brede, B.; Lau, A.; Herold, M.; McNicol, I.M.; Mitchard, E.T.A.; Coombes, D.; Jackson, T.D.; Makaga, L.; Milamizokou Napo, H.O.; Ngomanda, A.; Ntie, S.; Medjibe, V.; Dimbonda, P.; Soenens, L.; Daelemans, V.; Proux, L.; Nilus, R.; Labrière, N.; Jeffery, K.; Burslem, D.F.R.P.; Clewley, D.; Moffat, D.; Qie, L.; Bartholomeus, H.; Vincent, G.; Barbier, N.; Derroire, G.; Abernethy, K.; Scipal, K.; Disney, M. (2025): ForestScan Project : Terrestrial Laser Scanning (TLS) of FBRMS-03: Kabili-Sepilok, Malaysian Borneo 1ha plot SEP-30, March 2017. NERC EDS Centre for Environmental Data Analysis, <i>28 March 2025</i>. DOI:10.5285/ff217c783e3f4c66a4891d2b5807ee6e.</p>

		<a href="https://dx.doi.org/10.5285/ff217c783e3f4c66a4891d2b5807ee6e">https://dx.doi.org/10.5285/ff217c783e3f4c66a4891d2b5807ee6e</a>
Airborne LiDAR and RGB imagery from Sepilok Reserve and Danum Valley in Malaysia  Acquisition date: Feb 2020  License type: OGL UK 3.0 <a href="https://www.nationalarchives.gov.uk/doc/open-government-licence/version/3/">https://www.nationalarchives.gov.uk/doc/open-government-licence/version/3/</a>	<a href="#">ALS</a>	Coomes, D.A.; Jackson, T.D. (2022): Airborne LiDAR and RGB imagery from Sepilok Reserve and Danum Valley in Malaysia in 2020. NERC EDS Centre for Environmental Data Analysis, <i>03 October 2022</i> . DOI:10.5285/dd4d20c8626f4b9d99bc14358b1b50fe. <a href="https://dx.doi.org/10.5285/dd4d20c8626f4b9d99bc14358b1b50fe">https://dx.doi.org/10.5285/dd4d20c8626f4b9d99bc14358b1b50fe</a>
ForestScan: Tree census data for FBRMS-03: Kabili-Sepilok, Malaysian Borneo, plots SEP-11, SEP-12 and SEP-30  Acquisition date: SEP-11: Jan 2020 SEP-12: Mar 2020 SEP-30: Jun 2021  License: CC BY-NC-SA 4.0 <a href="http://creativecommons.org/licenses/by-nc-sa/4.0/">http://creativecommons.org/licenses/by-nc-sa/4.0/</a>	Tree census	Chavana-Bryant, C., Wilkes, P., Yang, W., Burt, A., Vines, P., Bennett, A.C., Pickavance, G., Cooper, D.L.M., Lewis, S.L., Phillips, O.L., Brede, B., Lau, A., Herold, M., McNicol, I.M., Mitchard, E.T.A., Barbier, N., Vincent, G., Coomes, D.A., Jackson, T., Makaga, L., Milamizokou Napo, H.O., Ngomanda, A., Ntie, S., Medjibe, V., Dimbonda, P., Soenens, L., Daelemans, V., Bartholomeus, H., Majalap, N., Nilus, R., Labrière, N., Burslem, D.F.R.P., Qie, L., Derroire, G., Proux, L., Abernethy, K., Jeffery, K., Clewley, D., Moffat, D., Scipal, K. and Disney, M. ForestScan: a unique multiscale dataset of tropical forest structure across 3 continents including terrestrial, UAV and airborne LiDAR and in-situ forest census data. ESSD. 2025 DOI: <a href="https://doi.org/10.5521/forestplots.net/2025_2">10.5521/forestplots.net/2025_2</a> <a href="https://doi.org/10.5521/forestplots.net/2025_2">https://doi.org/10.5521/forestplots.net/2025_2</a>

1016 **6. Author contributions**

Deleted: 1

1017 All authors provided input towards the writing of this manuscript.

1018 C.Ch.-B. wrote the manuscript with significant input from M.D.

1019 C.Ch.-B. developed the TLS data processing pipeline.

1020 C.Ch.-B. collected, cleaned, processed and curated TLS data.

1021 C.Ch.-B. developed the data repositories and ensured data integrity with support from M.D., the CEDA data management team

1022 and the ForestPlots and DataVerse database management teams.

1023 P.W. developed the TLS data processing pipeline, assisted in the collection of TLS data in FBRMS-02: Lopé, Gabon and its

1024 processing.

1025 W.Y. developed the TLS data processing pipeline, assisted in the collection of TLS data in FBRMS-01 Paracou, French Guiana

1026 and its processing.

1027 A.B., and T.J. collected TLS data in FBRMS-03: Kabili-Sepilok, Malaysian Borneo.

1031 H.O.M.N. and L.M. provided field logistics and assisted in the collection of TLS data in FBRMS-02: Lopé, Gabon  
1032 L.S. and V. D. helped collect TLS in FBRMS-02: Lopé, Gabon.  
1033 K.A., S.N. & A.N. provided logistics and research permit support for FBRMS-02: Lopé, Gabon.  
1034 P.V. assisted in the processing of TLS data and developing the TLS2trees Processing Scripts.  
1035 A.C.B. collected census data in FBRMS-01 Paracou, French Guiana and in FBRMS-02: Lopé, Gabon with assistance from  
1036 D.L.M.C.  
1037 V.M., P.D, H.O.M.N. and K.J collected the field census data for LPG-01  
1038 N.L., P.D., H.O.M.N. and K.J. collected the field census data for OKO-01, OKO-02 and OKO-03 in Lopé, Gabon.  
1039 T.J., D.C. and G.V. planned and funded the ALS data collection in FBRMS-01, Paracou French Guiana.  
1040 T.J. & D.C. planned and funded the ALS data collection in FBRMS-03, Kabili-Sepilok, Malaysian Borneo.  
1041 I.M.M. arranged, collected and processed the UAV-LS data collected over FBRMS-02: Lopé, Gabon.  
1042 B.B., A.L. and H.B. collected, cleaned, processed and curated TLS and UAV-LS data collected at Paracou, French Guiana.  
1043 N.B., G.V. collected, cleaned, processed and curated TLS and UAV-LS data collected at Paracou, French Guiana.

1044 **7. Competing interests**

1045 A.B. is an employee and/or shareowner of Sylvera Ltd. All other authors declare that they have no conflict of interest.

1046 **8. Acknowledgements**

1047 We are indebted to the long-term work of many researchers in funding, establishing and maintaining the field plots that were  
1048 used in this study. It is not possible to carry out meaningful cal/val measurements of tropical forest biomass for earth  
1049 observation studies without the logistical support and expertise of the plot PIs and their teams. We thank Dr Noreen Majalap  
1050 for logistical and research permit support in FBRMS-03, Kabili-Sepilok, Malaysian Borneo. We also thank the Sabah  
1051 Biodiversity Council for their support with airborne laser scanning data collection in Kabili-Sepilok, access license number:  
1052 JKM/MBS.1000-2/2 JLD.9 (122). We thank Esther Conway and her team for their outstanding support in developing the  
1053 ForestScan CEDA dataset collection. We thank Dr Aurora Levesley and Gaëlle Jaouen for their generous support in developing  
1054 the ForestPlots and DataVerse tree census data packages. Specific data collection activities were funded by the European Space  
1055 Agency under ESA/ contract No. 4000126857/20/NL/AI. Work in French Guiana benefited from the Investissement d'Avenir  
1056 grants of the ANR, France (CEBA: ANR-10-LABX-0025). M.D., P.W., C.Ch.-B., W.Y. acknowledge capital funding for TLS  
1057 equipment from UCL Geography and the NERC National Centre for Earth Observation (NCEO). T.J. and D.C. acknowledge  
1058 the funding for ALS data collection over FBRMS-01 Paracou, French Guiana in 2019 and FBRMS-03: Kabili-Sepilok,  
1059 Malaysian Borneo during February 2020 as part of a NERC project grant (NE/S010750/1). I.M.M. was partly funded by a

1060 European Research Council Starting Grant (757526) awarded to E.T.A.M. Work in Lopé was supported by core funding from  
1061 Total Gabon and the EU-ACP ECOFAC VI grant to the Gabon National Parks Agency for logistics, staff and site operations.

**Deleted:** ¶

1063 9. References

1064 R package Geomorph: Geometric Morphometric Analyses of 3D Data: <https://rdrr.io/cran/geomorph/man/read.ply.html>, last access: November 2025. Formatted: Space After: 6 pt

1065

1066 Agence Nationale des Parcs Nationaux (ANPN): Parcs Gabon, Recherche Scientifique: <https://scienceparcs gabon.weebly.com/>, last access: November 2024.

1067

1068 Arrizza, S., Marras, S., Ferrara, R., and Pellizzaro, G.: Terrestrial Laser Scanning (TLS) for tree structure studies: a review of methods for wood-leaf classifications from 3D point clouds, *Remote Sens Appl*, 36, 101364, ARTN 101364

1069

1070 10.1016/j.rsase.2024.101364, 2024.

1071 Askne, J. and Santoro, M.: Experiences in boreal forest stem volume estimation from multitemporal C-band InSAR, in: *Recent Interferometry Applications in Topography and Astronomy*, 169-194, 2012.

1072

1073 Avitabile, V., Herold, M., Henry, M., and Schmullius, C.: Mapping biomass with remote sensing: a comparison of methods for the case study of Uganda, *Carbon balance and management*, 6, 1-14, 10.1186/1750-0680-6-7, 2011.

1074

1075 Avitabile, V., Herold, M., Heuvelink, G. B., Lewis, S. L., Phillips, O. L., Asner, G. P., Armston, J., Ashton, P. S., Banin, L., and Bayol, N.: An integrated pan-tropical biomass map using multiple reference datasets, *Global change biology*, 22, 1406-1420, 10.1111/gcb.13139, 2016.

1076

1077

1078 Brede, B., Bartholomeus, H. M., Barbier, N., Pimont, F., Vincent, G., and Herold, M.: Peering through the thicket: Effects of UAV LiDAR scanner settings and flight planning on canopy volume discovery, *International Journal of Applied Earth Observation and Geoinformation*, 114, 103056, 10.1016/j.jag.2022.103056, 2022b.

1079

1080

1081 Brede, B., Terryn, L., Barbier, N., Bartholomeus, H. M., Bartolo, R., Calders, K., Derroire, G., Moorthy, S. M. K., Lau, A., and Levick, S. R.: Non-destructive estimation of individual tree biomass: Allometric models, terrestrial and UAV laser scanning, *Remote Sensing of Environment*, 280, 113180, 10.1016/j.rse.2022.113180, 2022a.

1082

1083

1084 Burt, A., Disney, M., and Calders, K.: Extracting individual trees from lidar point clouds using treeseg, *Methods in Ecology and Evolution*, 10, 438-445, 10.1111/2041-210x.13121, 2019.

1085

1086 Burt, A., Calders, K., Cuni-Sánchez, A., Gómez-Dans, J., Lewis, P., Lewis, S. L., Malhi, Y., Phillips, O. L., and Disney, M.: Assessment of bias in pan-tropical biomass predictions, *Frontiers in Forests and Global Change*, 3, 12, 10.3389/ffgc.2020.00012, 2020.

1087

1088 Calders, K., Verbeeck, H., Burt, A., Origo, N., Nightingale, J., Malhi, Y., Wilkes, P., Raumonen, P., Bunce, R. G., and Disney, M.: Laser scanning reveals potential underestimation of biomass carbon in temperate forest, *Ecological Solutions and Evidence*, 3, e12197, 10.1002/2688-8319.12197, 2022.

1089

1090

1091

1092 Chavana-Bryant, C., Wilkes, P., Yang, W., Burt, A., Bennett, A. C., Pickavance, G., Cooper, D., Lewis, S. L., Phillips, O. L., Brede, B., Herold, M., McNicol, I. M., Mitchard, E., Barbier, N., Vincent, G., Coomes, D. A., Jackson, T. D., Makaga, L., Milamizokou Napo, H. O., Ngomanda, A., Ntie, S., Medjibe, V., Dimbonda, P., Soenens, L., Daelemans, V., Bartholomeus, H., Majalap, N., Nilus, R., Labrière, N., Burslem, D. F. R. P., Qie, L., Derroire, G., Proux, L., Abernethy, K., Clewley, D., Moffat, D., Scipal, K., Vines, P., and Disney, M.: ForestScan: a multiscale dataset of tropical forest structure across 3 continents including terrestrial, UAV and airborne LiDAR and in-situ forest census data [dataset], 10.5285/88a8620229014e0ebacf0606b302112d, 2025.

1093

1094

1095

1096

1097

1098

1099 Chave, J., Réjou-Méchain, M., Bürquez, A., Chidumayo, E., Colgan, M. S., Delitti, W. B., Duque, A., Eid, T., Fearnside, P. M., and Goodman, R. C.: Improved allometric models to estimate the aboveground biomass of tropical trees, *Global change biology*, 20, 3177-3190, 10.1111/gcb.12629, 2014.

1100

1101

1102 Contributors, P.: PDAL VoxelCenterNearestNeighbor filter, PDAL documentation, available at: [code], 2025.

1|103 Cuni-Sanchez, A., White, L. J., Calders, K., Jeffery, K. J., Abernethy, K., Burt, A., Disney, M., Gilpin, M., Gomez-Dans, J.  
1104 L., and Lewis, S. L.: African savanna-forest boundary dynamics: a 20-year study, *PLoS One*, 11, e0156934,  
1105 10.1371/journal.pone.0156934, 2016.

1|106 de Lima, R. A., Phillips, O. L., Duque, A., Tello, J. S., Davies, S. J., de Oliveira, A. A., Muller, S., Honorio Coronado, E. N.,  
1107 Vilanova, E., and Cuni-Sanchez, A.: Making forest data fair and open, *Nature Ecology & Evolution*, 6, 656-658,  
1108 10.1038/s41559-022-01738-7, 2022.

1|109 Demol, M., Calders, K., Krishna Moorthy, S. M., Van den Bulcke, J., Verbeeck, H., and Gielen, B.: Consequences of vertical  
1110 basic wood density variation on the estimation of aboveground biomass with terrestrial laser scanning, *Trees*, 35, 671-684,  
1111 10.1007/s00468-020-02067-7, 2021.

1|112 Demol, M., Aguilar-Amuchastegui, N., Bernotaite, G., Disney, M., Duncanson, L., Elmendorp, E., Espejo, A., Furey, A.,  
1113 Hancock, S., and Hansen, J.: Multi-scale lidar measurements suggest miombo woodlands contain substantially more carbon  
1114 than thought, *Communications Earth & Environment*, 5, 366, 10.1038/s43247-024-01448-x, 2024.

1|115 Demol, M., Verbeeck, H., Gielen, B., Armston, J., Burt, A., Disney, M., Duncanson, L., Hackenberg, J., Kukenbrink, D., Lau,  
1116 A., Ploton, P., Sewdien, A., Stovall, A., Takoudjou, S. M., Volkova, L., Weston, C., Wortel, V., and Calders, K.: Estimating  
1117 forest above-ground biomass with terrestrial laser scanning: Current status and future directions, *Methods in Ecology and  
1118 Evolution*, 13, 1628-1639, 10.1111/2041-210x.13906, 2022.

1|119 Derroire, G., Hérault, B., Rossi, V., Blanc, L., Gourlet- Fleury, S., and Schmitt, L.: Paracou forest permanent plots (V3),  
1120 CIRAD Dataverse [dataset], 10.18167/DVN1/8G8AHY, 2023.

1|121 Derroire, G., Hérault, B., Rossi, V., Blanc, L., Gourlet-Fleury, S., and Schmitt, L.: ForestScan (DRAFT VERSION), CIRAD  
1122 Dataverse [dataset], doi/10.18167/DVN1/94XHID, 2025.

1|123 Open3D library: [https://www.open3d.org/docs/0.9.0/tutorial/Basic/file\\_io.html#mesh](https://www.open3d.org/docs/0.9.0/tutorial/Basic/file_io.html#mesh), last access: November 2025.

1|124 Duncanson, L., Armston, J., Disney, M., Avitabile, V., Barbier, N., Calders, K., Carter, S., Chave, J., Herold, M., and Crowther,  
1125 T. W.: The importance of consistent global forest aboveground biomass product validation, *Surveys in geophysics*, 40, 979-  
1126 999, 10.1007/s10712-019-09538-8, 2019.

1|127 Duncanson, L., Kellner, J. R., Armston, J., Dubayah, R., Minor, D. M., Hancock, S., Healey, S. P., Patterson, P. L., Saarela,  
1128 S., and Marselis, S.: Aboveground biomass density models for NASA's Global Ecosystem Dynamics Investigation (GEDI)  
1129 lidar mission, *Remote Sensing of Environment*, 270, 112845, 10.1016/j.rse.2021.112845, 2022.

1|130 Editorial: We must get a grip on forest science-before it's too late, *Nature*, 608, 449, 10.1038/d41586-022-02182-0, 2022.

1|131 Fischer, F. J., Jackson, T., Vincent, G., and Jucker, T.: Robust characterisation of forest structure from airborne laser  
1132 scanning—A systematic assessment and sample workflow for ecologists, *Methods in ecology and evolution*, 15, 1873-1888,  
1133 10.1111/2041-210x.14416, 2024.

1|134 ForestPlots.net, Blundo, C., Carilla, J., Grau, R., Malizia, A., Malizia, L., Osinaga-Acosta, O., Bird, M., Bradford, M.,  
1135 Catchpole, D., and Ford, A.: Taking the pulse of Earth's tropical forests using networks of highly distributed plots, *Biological  
1136 Conservation*, 260, 108849, 10.1016/j.biocon.2020.108849, 2021.

1|137 RIEGL Laser Measurement Systems GmbH: <https://www.riegl.co.uk/>, last access: 01/01/2025.

1|138 Goodman, R. C., Phillips, O. L., and Baker, T. R.: The importance of crown dimensions to improve tropical tree biomass  
1139 estimates, *Ecological Applications*, 24, 680-698, 10.1890/13-0070.1, 2014.

1|140 Jackson, T. D., Fischer, F. J., Vincent, G., Gorgens, E. B., Keller, M., Chave, J., Jucker, T., and Coomes, D. A.: Tall Bornean  
1141 forests experience higher canopy disturbance rates than those in the eastern Amazon or Guiana shield, *Global Change Biology*,  
1142 30, e17493, 10.1111/gcb.17493, 2024.

1|143 Jucker, T., Caspersen, J., Chave, J., Antin, C., Barbier, N., Bongers, F., Dalponte, M., van Ewijk, K. Y., Forrester, D. I., and  
1144 Haeni, M.: Allometric equations for integrating remote sensing imagery into forest monitoring programmes, *Global change  
1145 biology*, 23, 177-190, 10.1111/geb.13388, 2017.

1|146 Kellner, J. R., Armston, J., Birrer, M., Cushman, K., Duncanson, L., Eck, C., Fallegger, C., Imbach, B., Král, K., and Krúček,  
1147 M.: New opportunities for forest remote sensing through ultra-high-density drone lidar, *Surveys in Geophysics*, 40, 959-977,  
1148 10.1007/s10712-019-09529-9, 2019.

1|149 Krisanski, S., Taskhiri, M. S., Gonzalez Aracil, S., Herries, D., and Turner, P.: Sensor agnostic semantic segmentation of  
1150 structurally diverse and complex forest point clouds using deep learning, *Remote Sensing*, 13, 1413, 10.3390/rs13081413,  
1151 2021.

1|152 Labrière, N., Davies, S. J., Disney, M. I., Duncanson, L. I., Herold, M., Lewis, S. L., Phillips, O. L., Quegan, S., Saatchi, S.  
1153 S., and Schepaschenko, D. G.: Toward a forest biomass reference measurement system for remote sensing applications, *Global  
1154 Change Biology*, 29, 827-840, 10.1111/geb.16497, 2023.

1|155 Lopez-Gonzalez, G., Lewis, S. L., Burkitt, M., and Phillips, O. L.: ForestPlots.net: a web application and research tool to  
1156 manage and analyse tropical forest plot data, *Journal of Vegetation Science*, 22, 610-613, 10.1111/j.1654-1103.2011.01312.x,  
1157 2011.

1|158 Malhi, Y., Girardin, C., Metcalfe, D. B., Doughty, C. E., Aragão, L. E., Rifai, S. W., Oliveras, I., Shenkin, A., Aguirre-  
1159 Gutiérrez, J., and Dahlsjö, C. A.: The Global Ecosystems Monitoring network: Monitoring ecosystem productivity and carbon  
1160 cycling across the tropics, *Biological Conservation*, 253, 108889, 10.1016/j.biocon.2020.108889, 2021.

1|161 Martin-Ducup, O., Mofack, G., Wang, D., Raunonen, P., Ploton, P., Sonké, B., Barbier, N., Couteron, P., and Péliissier, R.:  
1162 Evaluation of automated pipelines for tree and plot metric estimation from TLS data in tropical forest areas, *Annals of botany*,  
1163 128, 753-766, 10.1093/aob/mcab051, 2021.

1|164 McNicol, I. M., Mitchard, E. T., Aquino, C., Burt, A., Carstairs, H., Dassi, C., Modinga Dikongo, A., and Disney, M. I.: To  
1165 what extent can UAV photogrammetry replicate UAV LiDAR to determine forest structure? A test in two contrasting tropical  
1166 forests, *Journal of Geophysical Research: Biogeosciences*, 126, e2021JG006586, 10.1029/2021JG006586, 2021.

1|167 Momo, S. T., Ploton, P., Martin-Ducup, O., Lehnebach, R., Fortunel, C., Sagang, L. B. T., Boyemba, F., Couteron, P., Fayolle,  
1168 A., and Libalah, M.: Leveraging signatures of plant functional strategies in wood density profiles of African trees to correct  
1169 mass estimations from terrestrial laser data, *Scientific Reports*, 10, 2001, 10.1038/s41598-020-58733-w, 2020.

1|170 Morhart, C., Schindler, Z., Frey, J., Sheppard, J. P., Calders, K., Disney, M., Morsdorf, F., Raunonen, P., and Seifert, T.:  
1171 Limitations of estimating branch volume from terrestrial laser scanning, *European Journal of Forest Research*, 143, 687-702,  
1172 10.1007/s10342-023-01651-z, 2024.

1|173 Ochiai, O., Poulter, B., Seifert, F. M., Ward, S., Jarvis, I., Whitcraft, A., Sahajpal, R., Gilliams, S., Herold, M., and Carter, S.:  
1174 Towards a roadmap for space-based observations of the land sector for the UNFCCC global stocktake, *Iscience*, 26, 106489,  
1175 10.1016/j.isci.2023.106489, 2023.

1|176 QGIS Geographic Information System: <https://qgis.org>, last access: November 2025.

1|177 Quegan, S., Le Toan, T., Chave, J., Dall, J., Exbrayat, J.-F., Minh, D. H. T., Lomas, M., D'alessandro, M. M., Paillou, P., and  
1178 Papathanassiou, K.: The European Space Agency BIOMASS mission: Measuring forest above-ground biomass from space,  
1179 *Remote Sensing of Environment*, 227, 44-60, 10.1016/j.rse.2019.03.032, 2019.

1|180 Ramachandran, N., Saatchi, S., Tebaldini, S., d'Alessandro, M. M., and Dikshit, O.: Mapping tropical forest aboveground  
1181 biomass using airborne SAR tomography, *Scientific Reports*, 13, 6233, 10.1038/s41598-023-33311-y, 2023.

1|182 Raunonen, P., Kaasalainen, M., Åkerblom, M., Kaasalainen, S., Kaartinen, H., Vastaranta, M., Holopainen, M., Disney, M.,  
1183 and Lewis, P.: Fast automatic precision tree models from terrestrial laser scanner data, *Remote Sensing*, 5, 491-520,  
1184 10.3390/rs5020491, 2013.

1|185 Roussel, J.-R., Auty, D., Coops, N. C., Tompalski, P., Goodbody, T. R. H., Sánchez Meador, A., Bourdon, J.-F., de Boissieu, 1186 F., and Achim, A.: lidR: An R package for analysis of Airborne Laser Scanning (ALS) data, *Remote Sensing of Environment*, 1187 251, 112061, <https://doi.org/10.1016/j.rse.2020.112061>, 2020.

1|188 Saatchi, S., Chave, J., Labrière, N., Barbier, N., Réjou-Méchain, M., Ferraz, A., and Tao, S.: AfriSAR: Aboveground Biomass 1189 for Lope, Maboum, Mondah, and Rabi Sites, Gabon [dataset], 10.3334/ORNLDAA/1681, 2019.

1|190 Saatchi, S. S., Harris, N. L., Brown, S., Lefsky, M., Mitchard, E. T., Salas, W., Zutta, B. R., Buermann, W., Lewis, S. L., and 1191 Hagen, S.: Benchmark map of forest carbon stocks in tropical regions across three continents, *Proceedings of the national 1192 academy of sciences*, 108, 9899-9904, 10.1073/pnas.1019576108, 2011.

1|193 Sabah Forestry Department: Official Website: <https://forest.sabah.gov.my/>, last access: 14/01/2025.

1|194 Schepaschenko, D., Chave, J., Phillips, O. L., Lewis, S. L., Davies, S. J., Réjou-Méchain, M., Sist, P., Scipal, K., Perger, C., 1195 and Herault, B.: The Forest Observation System, building a global reference dataset for remote sensing of forest biomass, 1196 *Scientific data*, 6, 198, 10.1038/s41597-019-0196-1, 2019.

1|197 CloudCompare (3D point cloud and mesh processing software) version 2.13: <https://www.cloudcompare.org>, last access: 1198 November 2025.

1|199 Verhelst, T. E., Calders, K., Burt, A., Demol, M., D'hont, B., Nightingale, J., Terryn, L., and Verbeeck, H.: Implications of 1200 Pulse Frequency in Terrestrial Laser Scanning on Forest Point Cloud Quality and Individual Tree Structural Metrics, *Remote 1201 Sensing*, 16, 4560, 10.3390/rs16234560, 2024.

1|202 Vincent, G., Verley, P., Brede, B., Delaire, G., Maurent, E., Ball, J., Clocher, I., and Barbier, N.: Multi-sensor airborne lidar 1203 requires intercalibration for consistent estimation of light attenuation and plant area density, *Remote Sensing of Environment*, 1204 286, 113442, 10.1016/j.rse.2022.113442, 2023.

1|205 White, L., Rogers, M. E., Tutin, C. E., Williamson, E. A., and Fernandez, M.: Herbaceous vegetation in different forest types 1206 in the Lopé Reserve, Gabon: implications for keystone food availability, *African Journal of Ecology*, 33, 124-141, 1207 10.1111/j.1365-2028.1995.tb00788.x, 1995.

1|208 Wilkes, P. and Yang, W.: rxp-pipeline: Tools to transform RIEGL terrestrial LiDAR, Zenodo [code], 2025a.

1|209 Wilkes, P. and Yang, W.: mat2ply: Tools for converting QSM data to 3D PLY models., Zenodo [code], 2025b.

1|210 Wilkes, P., Krisanski, S., Clewley, D., Moffat, D., and Yang, W.: TLS2trees (Version 0.1) Zenodo [code], 2025.

1|211 Wilkes, P., Lau, A., Disney, M., Calders, K., Burt, A., de Tanago, J. G., Bartholomeus, H., Brede, B., and Herold, M.: Data 1212 acquisition considerations for terrestrial laser scanning of forest plots, *Remote Sensing of Environment*, 196, 140-153, 1213 10.1016/j.rse.2017.04.030, 2017.

1|214 Wilkes, P., Disney, M., Armston, J., Bartholomeus, H., Bentley, L., Brede, B., Burt, A., Calders, K., Chavana-Bryant, C., 1215 Clewley, D., Duncanson, L., Forbes, B., Krisanski, S., Malhi, Y., Moffat, D., Origo, N., Shenkin, A., and Yang, W. X.: 1216 TLS2trees: A scalable tree segmentation pipeline for TLS data, *Methods in Ecology and Evolution*, 14, 3083-3099, 1217 10.1111/2041-210x.14233, 2023.

1|218 Zanne, A. E., Lopez-Gonzalez, G., Coomes, D. A., Ilic, J., Jansen, S., Lewis, S. L., Miller, R. B., Swenson, N. G., Wiemann, 1219 M. C., and Chave, J.: Global wood density database [dataset], 10.5061/dryad.234, 2009.

1220